Chrono-stratigraphy of the youngest (last 1500 years) rhyolitic eruptions of Lipari (Aeolian Islands, Southern Italy) and implications for distal tephra correlations

Chrono-stratigraphy of the youngest (last 1500 years) rhyolitic eruptions of Lipari (Aeolian Islands, Southern Italy) and implications for distal tephra correlations

M. Pistolesi[1,*] pistolesi@dst.unipi.it, M. Rosi[1], A.B. Malaguti[2], F. Lucchi[3], C.A. Tranne[3], F. Speranza[4], P.G. Albert[5,6], V.C. Smith[6], A. Di Roberto[7], E. Billotta[8]

[1]Dipartimento di Scienze della Terra, Università di Pisa, 56126 Pisa, Italy

[2]Dipartimento di Scienze Pure e Applicate, Università degli studi di Urbino Carlo Bo, 61029 Urbino, Italy

[3]Dipartimento di Scienze Biologiche, Geologiche e Ambientali, Università di Bologna, 40126 Bologna, Italy

[4]Istituto Nazionale di Geofisica e Vulcanologia, Sezione di Roma 2, 00143 Roma, Italy

[5]Department of Geography, Swansea University, College of Science and Engineering, Swansea, SA2 8PP, UK

[6]Research Laboratory for Archaeology and the History of Art, School of Archaeology, University of Oxford, Oxford OX1 3TG, UK

[7]Istituto Nazionale di Geofisica e Vulcanologia - Sezione di Pisa, 56126 Pisa, Italy

[8]Dipartimento di Scienze della Terra e Geoambientali, Università degli Studi di Bari "Aldo Moro", 70125, Bari, Italy

[*]Corresponding author.

Abstract

The youngest (last 1500 years) volcanic eruptions of Lipari, within the Aeolian Archipelago, produced the prominent pumice cone of Monte Pilato and the obsidian lava flows of Rocche Rosse and Forgia Vecchia, concentrated in the north-eastern sector of the island as well as highly dispersed white-colored, fine-grained tephra layers of rhyolitic composition in terrestrial and

marine settings on the regional scale. Here we describe in detail the stratigraphy of pyroclastic successions and lava flows erupted by different vents - Monte Pilato, Forgia Vecchia, Lami, and Rocche Rosse - combining field observations, sedimentological characteristics of the tephra deposits, and major and trace element compositions of the volcanic glass. All the pyroclastic materials consist of aphyric pumice lapilli and ash with a largely homogeneous rhyolitic composition. The Monte Pilato and Forgia Vecchia deposits primarily consist of highly vesicular pumice fragments and subordinate obsidian clasts, whilst Rocche Rosse and Lami are characterized by moderately vesicular juvenile fragments with a more significant fraction of obsidian. The Lami tephra also contains peculiar pumice clasts with a fibrous texture and breadcrust bombs.

Stratigraphic relationships, and paleomagnetic and ^{14}C ages of the lava and pyroclastic deposits are combined with the archaeological information and historical reports, enabling us to provide an accurate chrono-stratigraphic framework for the youngest eruptions of Lipari. Following the 8th century AD eruption of Monte Pilato, which produced a pumice cone and a obsidian lava flow, activity resumed in the second half of 13th century AD with the explosive eruption of Forgia Vecchia that culminated in the emission of a bilobate obsidian lava flow. This eruption was shortly followed by the explosive eruptions of Lami and Rocche Rosse, the latter concluded with the emission of the widely renowned obsidian lava flow.

By integrating stratigraphy and geochemistry of tephra deposits with a new chronological scheme, our work facilitates the refinement of proximal-to-distal correlation of Lipari's rhyolitic tephra in continental marine environments of the central Mediterranean area in the last 1,500 years. A fine-grained, rhyolitic ash found on Stromboli (~40 km NE from Lipari) has an origin from the Monte Pilato and thus, constrains tephra dispersion towards the NE. Very similar ash beds dispersed southwards and interlayered within the near-source deposits of La Fossa, Vulcano island (~10 km from Lipari) exhibit features that are consistent with the younger activities of the Rocche Rosse eruption. A possible link between previously identified rhyolitic ash layers

identified in marine cores of the Ionian Sea and the Forgia Vecchia eruption are postulated, although the age and textural characteristics of these distal tephra are not univocal in indicating a correlation to either Monte Pilato or Forgia Vecchia.

Keywords: Lipari; chrono-stratigraphy; rhyolitic eruption; paleomagnetism; tephra correlations

1. Introduction

Rhyolitic magmas have been erupted in the central sector of the Aeolian Islands (Lipari, Salina, Panarea and Vulcano) over the last 50 ka, generating the most powerful and intense explosive eruptions of the archipelago (De Rosa et al., 2003; Gioncada et al., 2003; Lucchi et al., 2007; De Astis et al., 2013; Forni et al., 2013; Lucchi et al., 2013a, b; Albert et al., 2017). During the last 1500 years, four rhyolitic eruptions took place on Lipari island from the vents of Monte Pilato, Forgia Vecchia, Lami and Rocche Rosse (Forni et al., 2013 and references therein; Fig. 1a). Several authors have studied the lava flows and pyroclastic products associated with these eruptions, including the globally renowned Rocche Rosse obsidian lava flow (Cas and Wright, 1987), and the Monte Pilato pumice cone (Dellino and La Volpe, 1995). However, the timing and proximal chrono-stratigraphic relationships between the different lava flows and pyroclastic deposits have remained in some respects controversial until now (Bigazzi and Bonadonna, 1973; Pichler, 1980; Cortese et al., 1986; Dellino and La Volpe, 1995; Keller, 2002; Bigazzi et al., 2003; Arrighi et al., 2006; Davì et al., 2009, 2011; Forni et al., 2013).

The accurate assessment of age and overall characteristics of rhyolitic tephra sourced from Lipari has direct implications for distal tephra correlations across the region (e.g., Albert et al., 2017) because all these explosive events were likely capable of generating airborne ash-sized material. Particularly widespread ash deposits from Lipari have been related to the early-Holocene Vallone del Gabellotto eruption (also known as the Gabellotto-Fiumebianco), tephra from this explosive activity is identified across the Aeolian archipelago, in marine sediments

from Tyrrhenian, Ionian and Adriatic Sea, along with the lacustrine sediment records and in the central Apennines (e.g. Albert et al., 2017; Di Roberto et al., 2018). Moreover, younger rhyolitic ash layers associated with the most recent cycle of explosive eruptions on Lipari (within the last 1500 yrs) also form time-stratigraphic markers found subaerially on Vulcano and Stromboli islands, whilst are recorded as both visible and cryptotephra within the marine sediments of the southern Tyrrhenian and Ionian Sea, and have even been traced as far as archaeological sites in Albania. These ash layers were generally correlated with the eruption of Monte Pilato, which for a long time was considered the only event from Lipari capable of producing ashes dispersed at great distances from the source area during the recent eruptive cycle (e.g. Albert et al, 2017). However, it is noteworthy that no detailed tephrostratigraphic study has been carried out to precisely connect the distal ash layers with the proximal deposits of the four different eruptions that occurred during the last 1500 years. This is crucial to better understand the timing and impact of Lipari's eruptive activity on the surrounding area, to date stratigraphic sequences, and to correlate and synchronize the palaeoclimatic, palaeoecological and archaeological archives. As an example, it is not clear whether the distal white rhyolitic tephra layers on Vulcano are attributed to the Monte Pilato, dated to AD 776 (Keller, 2002), or to the Rocche Rosse eruption that is dated to AD 1220 (Tanguy et al., 2003), which each provide different chrono-stratigraphic reconstructions of the La Fossa volcano (De Astis et al., 2013; Di Traglia et al., 2013; Fusillo et al., 2015; Rosi et al., 2018; Selva et al., 2020) and eruption frequency.

Here we document the pyroclastic successions (and lava flows) produced during eruptive activity in the last 1500 years on the island of Lipari, revising their stratigraphic relationships and providing details on their sedimentological, textural and geochemical features. The stratigraphic analysis of tephra is complemented by new ^{14}C and paleomagnetic dates of the different tephra units and associated lava flows, and a re-assessment of archaeological studies and historical reports (Manni et al., 2018). This revises the previous ages of the Monte Pilato, Forgia Vecchia, Rocche Rosse and Lami eruptions and constrains the chrono-stratigraphic relationships between

the different eruptions. The comparison of the physical and compositional features of the pyroclastic products are finally used to correlate the medial-distal tephra layers to their proximal source vents and hence, better constrain the magnitude and dispersal of the different eruptions.

2. Geological background, eruption chronology and distal occurrence of Lipari tephra

Lipari is the largest island of the Aeolian arc located in the southern Tyrrhenian Sea, Italy (Fig. 1). It is the emerged part of a large volcanic complex belonging to the Salina-Lipari-Vulcano volcanic belt that transversely intersects the archipelago in its central sector, aligned along the major NNW–SSE strike-slip Tindari–Letojanni fault system that controls magma rise and vent location (Barberi et al., 1994; Mazzuoli et al., 1995; Lanzafame and Bousquet, 1997; Billi et al., 2006; Ruch et al., 2016). Volcanic activity on the island developed between c. 267 ka and the Medieval Age (Bigazzi and Bonadonna, 1973; Pichler, 1980; Gillot, 1987; Crisci et al., 1991; De Rosa et al., 2003; Tanguy et al., 2003; Forni et al., 2013) and emplaced a large variety of lava flows and pyroclastic products that span a wide compositional range from basaltic andesites to rhyolites, all belonging to calc-alkaline and high-K calc-alkaline series (Pichler, 1980; Crisci et al., 1991; Gioncada et al., 2003; Di Martino et al., 2010; Forni et al., 2013, 2015; Albert et al., 2017).

According to the most recent geological maps (Forni et al., 2013; Lucchi et al., 2013c), the eruptive history of Lipari can be summarized into nine successive Eruptive Epochs, that span tens of thousands of years and are further subdivided into distinct eruptions or sequences of eruptions, separated by quiescence periods of variable duration. The last 1500 years of volcanic activity, which are the focus of this study, are included in the youngest Eruptive Epoch 9, which exclusively erupted rhyolitic pumiceous pyroclastic successions and obsidian lava flows in the north-eastern sector of the island. The earliest eruptions at c. 8.7-8.4 ka produced the widespread Vallone del Gabellotto pumiceous pyroclastic succession (cf. Vallone del Gabellotto Formation; Forni et al., 2013), characterized by a wide tephra fall distribution across distant islands of the

Aeolian archipelago and in marine sequences of the Tyrrhenian, Adriatic and Ionian Seas along with lacustrine records in the Central Apennines (Paterne et al., 1988; Siani et al., 2004; Di Roberto et al., 2008; Zanchetta et al., 2011; Lucchi et al., 2013; Albert et al., 2017; Di Roberto et al., 2018), and the associated obsidian-rich Pomiciazzo lava flow (cf. Pomiciazzo Formation; Forni et al., 2013). The youngest activity lies on a reddish palaeosol dated to between 5.5 and 1.2 cal. ka (^{14}C dates from Pichler (1980) were calibrated using IntCal20; Reimer et al., 2020) and comprises the eruptions of Monte Pilato, Forgia Vecchia, Lami and Rocche Rosse (Fig. 1a), which are the focus of this paper.

The Monte Pilato eruption produced a widespread thick pumiceous pyroclastic succession (cf. Sciarra dell'Arena Formation; Forni et al., 2013) and a final obsidian lava flow (cf. sa1 member; Forni et al., 2013) that are exposed along the northern rim of the Monte Pilato crater. This eruption is dated to AD 780 (AD 675-880) from the ^{14}C date of carbonized plant fragments contained within the basal portion of the pyroclastic succession (Keller, 2002; recalibrated here using IntCal20).

The Forgia Vecchia bilobate obsidian lava flow (cf. Forgia Vecchia Formation; Forni et al., 2013) was emitted from a low-profile crater in the area of Pirrera after the emplacement of a pumiceous, lithic-rich pyroclastic succession (cf. fv1 member; Forni et al., 2013; Fig. 1). The age of this eruption is controversial. The lava flow was fission-track dated to 1.6 ka (± 0.38) by Bigazzi and Bonadonna (1973), which implies that it was erupted before the Monte Pilato eruption. Forni et al. (2013) questioned this age attribution owing to the absence of the Monte Pilato pumiceous products above Forgia Vecchia deposits, and instead proposed that the eruptions of Forgia Vecchia and Monte Pilato were contemporaneous, which is in agreement with the interpretation by Cortese et al. (1986) that is based on the recognized interlayering of the corresponding pyroclastic successions.

The Rocche Rosse eruption occurred after a period of quiescence recorded by an erosional unconformity at the top of the Monte Pilato pyroclastic succession. The eruption ended with the

spectacular Rocche Rosse obsidian lava flow (cf. Fossa delle Rocche Rosse Formation; Forni et al., 2013), which outpoured from the northeastern rim and a low-profile crater, nested within the older Monte Pilato crater, where a pumiceous (obsidian), lithic-rich pyroclastic succession formed (cf. frr1 member; Forni et al., 2013). The Rocche Rosse lava flow was dated to 1.4 ka (± 0.45) by fission track (Bigazzi and Bonadonna, 1973). A younger age of AD 1220 (± 30) was proposed by Tanguy et al. (2003) using archeomagnetic dating, which is consistent with the stratigraphic finding of the Rocche Rosse products above an erosional unconformity in the Monte Pilato pyroclastic succession (Dellino and La Volpe, 1995; Forni et al., 2013).

The Lami eruption produced a lithic- and obsidian-rich pumiceous pyroclastic succession (cf. Lami Formation; Forni et al., 2013) with limited dispersal, which is located at the foot of the southern flank of Monte Pilato pumice cone, close to the village of Lami (Pichler, 1976; Cortese et al., 1986; Dellino, 1991; Lucchi et al., 2010; Forni et al., 2013). Davì et al. (2011) proposed that the Lami tephra was a part of the Monte Pilato pyroclastic succession, a view also put forward by Cortese et al. (1986) who suggested that the Lami and Monte Pilato activities were contemporaneous based on the interlayering of the corresponding products. Conversely, the Lami products are fission-track dated to AD 1250 (± 170) by Bigazzi et al. (2003), which is the preferred age adopted by Forni et al. (2013) based on stratigraphic and volcanological evidence.

Within the Aeolian archipelago, distal ash layers associated with the more recent eruptive cycle (last 1500 yrs) of Lipari have been found subaerially: i) interbedded within the products of the Commenda eruption deposits of the La Fossa cone on Vulcano island (Keller, 1980; De Astis et al., 2013; Gurioli et al. 2012; Di Traglia et al., 2013; Fusillo et al., 2015; Albert et al., 2017; Rosi et al., 2018), ii) at the base of the eruptive products of the present-day activity of Stromboli (Rosi et al., 2000, 2013). More distally, rhyolitic tephra and cryptotephra layers within the same time-stratigraphic window have been found in the southern Tyrrhenian Sea (Paterne et al., 1988; Di Roberto et al., 2008; Albert et al., 2012, 2017), in the Gulf of Taranto (Di Donato et al., 2019), and in the Ionian Sea (Caron et al., 2012; Menke et al., 2018; Insinga et al. 2020), in which they

represent important regional marker horizons. Several of these studies provide independent dating (^{14}C, oxygen-isotope data, ecostratigraphy, sedimentation rates) for the rhyolitic tephra layers found within the respective cores that will be used here to cross-check distal correlations.

3. Research strategy and methods

To achieve our goal reconstructing the sequence of eruptive activity in the last 1500 years on Lipari we adopted the following methods: i) field study of the lithological and sedimentological features of the Monte Pilato, Forgia Vecchia, Rocche Rosse and Lami tephra successions, and analysis of the stratigraphic relationships between the tephra units and the obsidian lava flows; (ii) sampling and laboratory analyses of textural, sedimentological and geochemical features of representative samples of the four tephra successions; iii) new dates (paleomagnetism and radiocarbon [^{14}C]) of the Lami and Rocche Rosse pyroclastic products, and the Forgia Vecchia tephra and lava flow units; iv) revision of the available geochronological information from archaeological studies and historical reports; v) comparison of the characteristics of rhyolitic distal fallout ash beds found on Stromboli and Vulcano islands to correlate them to their proximal counterparts on Lipari.

The overall stratigraphic architecture was reconstructed from 16 outcrops covering the whole north-eastern sector of the island of Lipari, with key sections along the ridge to the north of Forgia Vecchia and the southern flank of Monte Pilato where the Lami eruptive vent is located (Fig. 1a, b). A total of 43 representative samples, collected from the base to the top of each of the pyroclastic successions, were subject to textural, grain-size and componentry analyses in the Laboratorio di Petrologia e Vulcanologia at the Istituto Nazionale di Geofisica e Vulcanologia, Sezione di Pisa (INGV-Pisa). Samples were also collected of the rhyolitic distal fallout ash beds recognized on Vulcano and Stromboli islands, and these were analysed for comparison. Grain-size analyses were carried out with mechanical dry sieving at one-φ intervals from -4 to 6 φ ($\varphi = -\log_2 D$, where D is the particle diameter in millimeters). The main sedimentological parameters

of median and sorting (Mdϕ and σϕ, respectively) were calculated according to Inman (1952). Textural analyses were carried out with a scanning electron microscope (SEM) Zeiss EVO MA at the INGV-Pisa on juvenile clasts ranging in size from 250 to 500 μm belonging to ten samples representative of the four studied tephra successions. Componentry was studied under a binocular optical microscope, following a subdivision into five main classes: i) highly vesicular juvenile fragments; ii) weakly vesicular juvenile fragments; iii) fresh obsidian clasts, generally considered to belong to the juvenile fraction; iv) andesitic lithic clasts; and v) rhyolitic lithic clasts (including altered obsidian). Based on the assumption that the lithic material embedded within a pyroclastic succession provides information on the underlying deposits at the source area, we assessed for each of the studied pyroclastic successions the relative abundance of different lithic types by randomly hand-picking them at each outcrop c. 100 clasts with a diameter in the range of 5-10 cm. Most of them were broken directly in the field and observed with a hand lens to classify their lithology and composition, and to estimate the percentage of different lithotypes.

Glass geochemistry (major and trace elements) was performed on the juvenile fraction of 16 samples representative of the four studied proximal pyroclastic successions of Monte Pilato, Forgia Vecchia, Rocche Rosse and Lami. Chemical investigations were also carried out on glass fragments from the distal fallout rhyolitic ash beds that outcrop on Vulcano (Vulcanello) and Stromboli, which are considered chrono-stratigraphically relevant to the recent eruptions of Lipari (see Section 5). Major elements were analysed at the Research Laboratory of Archaeology and the History of Art, University of Oxford, using a JEOL 8600 electron microprobe (EMPA) operating at 15 kV accelerating voltage, 6 nA beam current, 10 micron probe diameter, counting times of the peaks 30 seconds for all the elements (except for the Na, for which they were 10 seconds). The MPI-DING reference glasses ATHO-G, StHs6/80-G and GOR132-G (Jochum et al., 2006) were used to monitor the accuracy and precision of the analyses. Trace element analyses of the volcanic glasses were performed using an Agilent 8900 triple quadrupole ICP-

MS (ICP-QQQ) coupled to a Resonetics 193nm ArF excimer laser-ablation in the Department of Earth Sciences, Royal Holloway, University of London. Complete analytical procedures for volcanic glass analysis are reported in Tomlinson et al. (2010). Analyses were conducted using a 34 μm spot for the proximal (and Vulcano) samples, and 25 μm for the distal tephra identified on Stromboli. The repetition rate was 5 Hz, with a count time of 40 seconds on the sample, and 40 seconds on the gas blank to allow the subtraction of the background signal. Typically groups of eight glass shards and one MPI-DING reference glass were bracketed by the NIST612 glass calibration standard. The internal standard used was ^{29}Si, determined by EMP analysis. In addition, MPI-DING reference glasses were used to monitor analytical accuracy (Jochum et al., 2006). LA-ICP-MS data reduction was performed in Microsoft Excel (Tomlinson et al., 2010). Accuracies of LA-ICP-MS analyses of the ATHO-G and StHs6/80-G MPI-DING glass were typically ≤5% for most elements measured. The full trace element glass dataset generated for the Lipari tephra samples analysed, along with analyses of the MPI-DING reference glasses, can be found in Supplementary Information. Major element glass data are reported and presented as normalised to 100% (water-free basis), while compositional averages are reported alongside their 2σ value, unless otherwise stated. Owing to the similarity in normalised major element compositions of the historical Lipari products, we have reported noticeable differences in analytical totals between some eruption deposits analysed, this is adopted as a qualitative means of inferring relative differences in H_2O (volatile) content between samples, in the absence of direct measurements. While we accept differences in analytical totals (reductions) can derive from secondary hydration, this is unlikely to be a significant issue in these very young, fresh terrestrial pyroclastic deposits, and this assumption is supported by the consistent analytical totals at an individual sample level.

Ages for the Forgia Vecchia, Lami and Rocche Rosse lava flows and pyroclastic deposits were obtained by paleomagnetic and accelerator mass spectrometry (AMS) radiocarbon dating. Paleomagnetic dating has been widely used in the last three decades to date recent volcanic

successions (e.g., Speranza et al., 2006, 2008; Di Chiara et al., 2012, 2014; Villasante-Marcos and Pavón-Carrasco, 2014; Greve and Turner, 2017; Juárez-Arriaga et al., 2018; Branca et al., 2019; Risica et al., 2019, 2020). In this study, we paleomagnetically dated the Forgia Vecchia and Rocche Rosse lava flows and welded pumice deposits of the Rocche Rosse and Lami pyroclastic successions. Eight sites were sampled, one for the Lami pyroclastic succession, three for the Forgia Vecchia lava flow, and four for the Rocche Rosse tephra and lava flow (Fig. 1a). The samples were collected using a water-cooled, petrol-powered portable drill. Ten to sixteen, 2.5 cm-diameter cores oriented in situ by both a sun and a magnetic compass were obtained from each of the eight sampling sites, and 91 cores were collected in total. The natural remanent magnetization (NRM) of one specimen per core was measured in the shielded room of the paleomagnetic laboratory of the Istituto Nazionale di Geofisica e Vulcanologia (Rome) by means of a 2G Enterprises direct current, super-conducting quantum interference device (SQUID) cryogenic magnetometer. All the samples were progressively subjected to alternating field (AF) cleaning (yielded by three coils online with the magnetometer), using 11 demagnetization-measurement steps (0 to 120 mT) per specimen. AF demagnetization data were plotted on both orthogonal diagrams (Zijderverd, 1967) and equal-area projections, and the magnetization components were isolated by means of a principal component analysis (Kirschvink, 1980). Site-mean paleomagnetic directions were obtained using standard Fisher statistics (Fisher, 1953). Paleomagnetic dates were established by comparing the mean paleomagnetic directions obtained for each lava and tephra unit with the recent reference curve of the geomagnetic field palaeo-secular variations (PSV) of Pavón-Carrasco et al. (2021; SCHA.DIF.4K), using the Matlab software by Pavón-Carrasco et al. (2011). The characteristic magnetization directions (ChRMs) for each sample gathered from the same volcanic unit were combined to get a unit-mean paleomagnetic direction that translated to a given age after comparison with the PSV model. The paleomagnetic direction from one site of Rocche Rosse lava already sampled by Arrighi et al. (2006) was re-dated using the updated reference PSV curve by Pavón-Carrasco et al. (2021).

The paleomagnetic dataset was integrated with two radiocarbon (^{14}C) age determinations from charred material sampled in the palaeosol immediately underlying the Forgia Vecchia tephra sequence. The charcoals were chemically pre-treated at the Oxford Radiocarbon Accelerator Unit (ORAU) using the acid-base-acid (ABA) methodology outlined by Brock et al. (2010). The ^{14}C analyses were acquired using a HVEE AMS system at ORAU (Ramsey et al., 2004). The radiocarbon ages were calibrated in OxCal v4.4 (Ramsey, 2009) using the IntCal20 calibration curve (Reimer et al., 2020) and are presented in calendar years AD.

4. Results

4.1. Stratigraphy and lithology

The lava flows and pyroclastic successions of Monte Pilato, Forgia Vecchia, Rocche Rosse and Lami are recognized in different sites of the northeastern sector of Lipari, showing distinctive lithological and sedimentological features. All of them sit on a reddish palaeosol that formed above the Vallone del Gabellotto pyroclastic succession (and Pomiciazzo lava flow), but direct stratigraphical relationships between the distinct units are generally difficult to recognize in the field due to the limited number of exposures. The main lithological, sedimentological and textural features of the studied units are hereafter described according to their chrono-stratigraphic order established in this work (starting from the oldest).

4.1.1. Monte Pilato

The Monte Pilato (MP) pumiceous pyroclastic succession is exposed in the north-eastern sector of the island of Lipari. The contact with underlying units is marked by an up to 0.5 m reddish to dark-coloured, humic-rich palaeosol. The MP deposits built a pumice cone that reaches a maximum height of c. 350 m with average slope angles of 20º-30º, and it has a 1 km large summit crater that is open to the NE (Fig. 1b). The pyroclastic succession is superbly exposed in the eastern sector of the cone in the up to ~150 m cliffs left by pumice quarries that were active

until the 1990's. These sections cut the flanks and crater of the pumice cone near Porticello and Acquacalda (Fig. 2a). The MP succession mainly consists of matrix-supported, massive to crudely stratified ash and lapilli beds of variable thickness, alternating with well-sorted, massive to normal-graded, clast-supported lapilli beds. White-coloured, highly vesicular pumice with spherical to elongated vesicles constitute up to 97 wt.% of the deposit. The remaining 3 wt. % is accounted by lithic clasts of andesitic lava (which represent up to 25 wt.% of the whole deposit in samples collected at the base of the sequence) with a minor component of rhyolitic lava (Table 1). The upper portion of the MP succession is progressively more stratified, and contains pumice clasts that become progressively less vesicular towards the top. The decrease in juvenile vesicularity is accompanied by a significant increase of obsidian clasts from the base (4 wt.%) to the top (15 wt.%; Fig. 3a, c) of the deposit. The amount of fine ash is particularly conspicuous in the upper portion where the F2 fraction (<63 μm) is up to 30 wt.%. The upper portion of MP is observed in the Acquacalda quarry, along the rim of the crater and in the locality of Capo Rosso that connects the villages of Canneto and Porticello (Fig. 1b), and has a thickness that varies between ~2 and 16 m.

Remnants of an obsidian lava flow are discontinuously recognized above the pyroclastic succession along the lower, north-eastern side of the MP crater (cf. Sciarra dell'Arena Formation, sa1 member; Forni et al., 2013). Unfortunately, dense vegetation and steep slopes made it impossible to access some sections for observations and sampling.

4.1.2. Forgia Vecchia

The most prominent deposit of the Forgia Vecchia (FV) activity, whose vent is located ~3 km south of Monte Pilato, is a bilobate, tongue-like (30 m thick), obsidian-rich lava flow with typical foliation structures. The blocky and cracked surface is observed hanging behind the Canneto village. The lava flow originated from the eastern rim of a low-profile, barely visible, tephra ring with a diameter of 500-600 m that is located near the village of Pirrera (Fig. 1a). The

FV tephra was described and sampled in two locations. The most proximal outcrop has a thickness of 5 m (base not exposed), whereas our most complete base-to-top exposure is about 2 m thick and is located ~600 m north of the crater, where the FV tephra is emplaced over a ~1 m-thick palaeosol formed above the Vallone del Gabellotto pyroclastic succession. The FV pyroclastic succession comprises medium to thick beds of massive, ash to clast-supported pumice lapilli and bombs and lithics with crude layering and overall normal grading. Some beds are plane parallel- to cross-stratified, but the majority of the deposit consists of clast-supported, pumice lapilli beds (Fig. 2d). Grain-size distributions of analysed samples show good to poor sorting ($\sigma\phi$ range 1.3-2.5), with unimodal curves displaying an excess of fine material (negative skewness) (Table 1). Tephra beds consist of juvenile rhyolitic whitish to grey pumice as the most abundant component (up to 89 wt.%; Fig. 4 and Table 1), and lithics of andesite lavas with a maximum size of 40 cm. Pumice clasts are generally highly vesicular and have an elongated shape. Towards the top, up to 50 cm in diameter obsidian blocks and breadcrust bombs are more abundant, with obsidian blocks creating impact sags. Black obsidian clasts get greyer in colour towards the top of the sequence and some of them are micro-vesicular.

At some localities, the FV lava flow is overlain by patches of an up to 15-20 cm thick, partially altered and hardened, thinly stratified, normal-graded deposit of whitish ash and lapilli that is rich in obsidian chips.

4.1.3. Rocche Rosse

The Rocche Rosse (RR) eruption produced the renowned lava flow that forms the north-eastern edge of the island of Lipari (Fig. 1b). It is a lobate, tongue-like (up to 60 m thick), obsidian-rich lava flow with developed ramps and flow foliation, and blocky and cracked surface (Shields et al., 2016; Bullock et al., 2018). The lava flow originates from the lowered north-eastern rim of a 30-m-high, low-profile tephra ring (400 m large in diameter), hosted within the older Monte Pilato crater, and it reaches the sea in the area between Porticello and Acquacalda. The RR

tephra succession is separated from the underlying MP deposits by an erosional unconformity visible at the top of the wall at the Porticello quarry, and by the slope detritus and reworked deposits near the basal MP flanks. The RR succession was examined and sampled in two main exposures, one along the rim of the tephra ring at the top of the Porticello quarry, and the other along the MP crater rim (Fig. 1a). The maximum observed thickness exceeds 10 m. The succession comprises multiple, medium to thick, clast-supported beds of lithic-rich, pumiceous lapilli that alternate with thin to medium beds of whitish ash and lapilli and include accretionary lapilli. Coarser bombs, often surrounded by halos of red oxidation, are also present. A distinctive m-thick layer of dark-coloured, welded, highly vesicular pumice fragments is observed in proximal outcrops (Fig. 2c). Grain-size features of loose deposits show moderately good ($\sigma\phi$=1.4) to poor ($\sigma\phi$=-3.0) sorting, with commonly asymmetric curves skewed toward the fine fractions. The juvenile fraction mostly consists of whitish to grey, moderately vesicular to dense juvenile clasts (up to 94 wt.%) and grey to black obsidians. Lithic clasts predominantly consist of rhyolite lavas with sporadic andesite lavas (Fig. 5a, c; Table 1).

4.1.4. Lami

The Lami (LA) pyroclastic succession is produced by a small vent located on the southern flank of the MP cone near the village of Lami. The best exposures are located in a small quarry and in a road cut near the village of Lami, where four stratigraphic sections were correlated to reveal a total unit thickness of ~12 m (Fig. 2b). The LA tephra constructed a low-profile pyroclastic cone around a crater dug in the Pomiciazzo lava flow and the MP deposits. This cone is presently largely eroded and dismantled by human activity and mining. The LA succession consists of thin to thick beds of medium- to well-sorted, clast-supported pumice lapilli and bombs beds that alternate with minor massive to stratified, ash-supported lapilli beds that include large blocks and several finer ash layers. There is a distinctive densely welded m-thick layer with flattened, highly vesicular pumice at the top of the succession (‘pipernoid pumice deposits’; Pichler, 1980). Most

of the succession is made up of distinctive whitish to grey, highly vesicular to frothy pumice with elongated to tubular vesicles, and grey and black to banded obsidian clasts and mixed pumice-obsidian clasts. Lithics only consist of pluri-dm angular clasts of rhyolitic lava (Table 1). Subordinate, dm-sized breadcrust bombs are present. Coarser clasts of rhyolite lava and obsidian are generally associated with impact sags. Grain-size features of representative samples show moderately good to poor sorting ($\sigma\phi$ ranging between 1.6-3.7), with asymmetric curves toward the finer material, and few exceptions of positive skewness (bimodal trends to coarser fractions) (Table 1).

In the lower part of the succession there are some interlayered beds of fine-grained, whitish ash with slightly different features (Fig. 6). In fact, whilst most of the LA tephra is made up of coarse-grained samples with unimodal grain-size curves, those beds are richer in fine material (F1 fraction <1 mm =39 wt.%) and show bimodal grain-size distributions, containing light grey to white, poorly vesicular to dense juvenile fragments, obsidian clasts and andesitic lithics.

Notably, a 30 cm layer of stratified ash and lapilli with the typical features of LA is recognized above the FV tephra in a key outcrop along the ridge that bounds to the south the Vallone del Gabellotto gorge. This LA outcrop includes breadcrust bombs and a N-to-S bomb-sag that is consistent with a provenance from the LA vent. At this locality, no alteration or evidence of erosion were observed between the FV and LA beds.

4.2. Geochemistry of the juvenile fraction

Major and trace element volcanic glass data are reported in Table 2 as sample compositional averages, whilst the complete dataset is provided in the Supplementary Information (Table S1). Major element glass compositions of all the studied samples are classified as rhyolites following the Total Alkali vs SiO_2 diagram (TAS; LeBas et al., 1986) (Figs. 3-6) and display a high-K calc-alkaline affinity (SiO_2 ~75 wt.% and K_2O ~5 wt.%) (Table 2).

The MP tephra glasses are homogeneous rhyolites (*n=129*) with 74.8 ± 0.5 wt.% SiO_2 and 9.2 ± 0.2 wt.% Na_2O+K_2O (Fig. 3b), and CaO and FeOt contents display limited variability with 0.7 ±

0.1 wt.% and 1.6 ± 0.2 wt.%, respectively. The average analytical total throughout the MP dataset is 96.7 ± 1.9 wt.% (1 s.d.) which allows us to infer significant H_2O contents in these young rhyolitic products.

The FV samples (*n=80*) are also homogeneous with SiO_2 contents of 75.4 ± 0.4 wt.%, Na_2O+K_2O contents of 9.1 ± 0.3 wt.% (Fig. 4b), and 0.7 ± 0.1 wt.% CaO and 1.5 ± 0.2 wt.% FeOt. The average analytical total for the FV glasses is 99.7 ± 1.0 wt. % (1 s.d.), higher than the totals of MP and suggesting a lower H_2O content than MP.

The RR tephra (*n=114*) glasses show subtly more SiO_2 variability than MP and FV products with SiO_2 contents of 73.5-75.8 wt.% (74.8 ± 0.9 wt.%) and Na_2O+K_2O contents of 8.7-9.6 wt.% (Fig. 5b). Whilst CaO (0.7 ± 0.1 wt.%) and FeOt (1.6 ± 0.2 wt.%) show very little compositional variability. Increases in SiO_2 content are accompanied by overall decreases in Al_2O_3 and K_2O contents. The average analytical totals for the RR glasses of 98.8 ± 1.3 wt. % (1 s.d.) are higher than those of MP, but lower than those of FV.

The LA tephra (*n=50*) shows restricted major element compositional variability with 75.3 ± 0.4 wt.% SiO_2, and Na_2O+K_2O contents of 9.1 ± 0.2 wt.% (Fig. 6b). CaO and FeOt contents are very homogeneous, with 0.7 ± 0.1 wt.% and 1.5 ± 0.2 wt.%, respectively. The average analytical total for the LA glasses is 99.3 ± 0.8 wt. % (1 s.d.), higher than those of MP and more akin to those of FV and RR (Table 2).

Overall, the major and minor element compositions of the four tephra deposits associated with the different eruptions are largely indistinguishable, particularly given the analytical uncertainty (Figs. 3-6; Table 2). The only notable differences are the consistently lower analytical totals associated with the MP glasses (Table 2), and the subtly higher SiO_2 variability in the RR glasses.

Similarly, the trace element compositions of the analysed tephra deposits overlap (Figs. 3-6; Fig. S1). Normalised to primitive mantle, the glasses all display identical profiles with pronounced depletions in Ba, Sr and Eu, which are consistent with K-feldspar fractionation (Fig. S1). Glasses

from all the four eruptions are enriched in the Light Rare Earth Elements (LREE) relative to the Heavy Rare Earth Elements (HREE; Fig. S1). Trace element concentrations of the FV, RR and LA volcanic glasses are all relatively homogeneous (Table 2), compositionally overlapping with the MP and one another. Conversely, most MP glasses show significantly greater trace element heterogeneity, with some MP glasses displaying distinctly lower levels of enrichment in incompatible elements (Figs. 3-6). This potentially diagnostic feature is well illustrated by comparing the Th content of the glasses associated with the different eruption deposits, highlighting that MP glasses span a larger range of 42.1-56.4 ppm Th compared to those of FV (52.3-56.9 ppm), RR (50.9-56.9 ppm) and LA (49.5-57.4 ppm) (Figs. 3-6). Interestingly, while some individual MP samples show a narrower trace element variability more consistent with FV, RR and LA compositions, most MP samples display greater variability, with these more heterogeneous samples displaying no clear relationship with juvenile texture and/or stratigraphic height throughout the investigated succession.

4.3. Dating

4.3.1. Radiocarbon (^{14}C) ages

Two radiocarbon age determinations were carried out on charcoal material embedded within the uppermost 5 cm of the palaeosol at the base of the FV tephra (Table S2). These charcoals yield ^{14}C ages of 842 ± 26 yrs (LIP1704A1; OxA-38,254) and 868 ± 25 yrs (LIP1704A2; OxA-38,282), which correspond to AD 1165-1265 and AD 1050-1255 (95.4%; IntCal20), respectively. Given that the charcoals were sampled at the same stratigraphic level, we combined the two radiocarbon ages to obtain a ^{14}C date of 856 ± 19 yrs BP, which calibrates to AD 1160-1260 (95.4%; IntCal20). This date is consistent with the younger dates of Pichler (1980) for the palaeosol set above the Vallone del Gabellotto pyroclastic succession, which is stratigraphically below the FV tephra. Consequently, an age younger than AD 1160-1260 is suggested for the FV tephra and lava flow.

4.3.2. Paleomagnetic dating

Four paleomagnetic dates are obtained for the RR lava flow and welded dark pumice, the FV lava flow, and the LA welded pumice deposit. A characteristic ChRM in the 20–120 mT AF interval was isolated for almost all the analysed samples (Fig. S2). NRM values are all similar and range mostly between 1 and 20 A/m, except for the LA pumice that yield NRM comprised between 0.08 and 0.3 A/m. Site-mean paleomagnetic declinations are in the 3.5°-18.3° range (Table 3, Fig. 7a), whilst inclinations are comprised between 29.0° and 52.9°. The α_{95} values relative to the site-mean paleomagnetic directions vary from 3.5° to 5.9° (4.7° on average). We discarded the incredibly scattered (a_{95} values >10°) paleomagnetic directions from the LIP01 and LIP06 sites belonging to the FV lava flow. Data scatter is likely due to local block rotation/tilt typical of a highly viscous rhyolitic lava flow. The paleomagnetic directions from the RR lava flow are consistent with those gathered from the same flow by Arrighi et al. (2006) and Lanza and Zanella (1991), and all of them show angular deviations within 10°.

Input age windows needed to obtain paleomagnetic dates were based on literature data and our stratigraphic observations. Regarding the FV lava flow, we used an AD 400-1500 age window that brackets both the fission track age of 1.6 ka (± 0.38) given by Bigazzi and Bonadonna (1973) and the new radiocarbon age provided in this work (younger than AD 1160-1260). For the RR lava flow and welded pumice we used an AD 700-1500 age window that encompasses the: i) ^{14}C date of AD 675-880 (Keller, 2002; Table S2) for the stratigraphically underlying MP pyroclastic succession, ii) ^{14}C date of AD 1320-1340 (0.61±0.02 ka) provided by Caron et al. (2012) for a cryptotephra sourced from Lipari in a marine core in the northern Ionian Sea; and iii) the archeomagnetic age of AD 1220 (± 30) proposed by Tanguy et al. (2003) for the RR lava flow. A similar age window of AD 700-1500 is adopted for the LA tephra bracketing the ^{14}C age of AD 675-880 for the stratigraphically older MP pyroclastic succession and the fission track age of 700 ± 170 years BP (AD 1080-1420) provided by Bigazzi et al. (2003).

Paleomagnetic dating of the FV lava flow (site LIP02) yields a date of AD 1242-1306 (Table 3; Figs. 7b and S3), which is chrono-stratigraphically consistent with the new ^{14}C date of AD 1160-1260 determined on charcoals from the underlying palaeosol. A paleomagnetic age of AD 1253-1316 is obtained for the LA welded pumice. We exclude the AD 1392-1410 date based on the low probability density peak (Table 3; Figs. 7b and S3). The RR welded pyroclastic material yields two possible ages - AD 1329-1417 and AD 1420-1490, and the date for the RR lava flow is AD 1243-1304 (Table 3; Figs. 7b and S3). The latter is corroborated by both our paleomagnetic directions, and the paleointensity value from the RR lava (52.4 ± 1.1 μT) reported by Leonhardt et al. (2006). Accordingly, we consider the AD 1243-1304 date obtained for the RR lava flow as reliable. The dates for the welded pyroclastic material yield scattered ages, which are probably related to the unstable nature of the deposits, which are more prone to fail and tilt after emplacement with respect to quasi-solid lava flows (e.g. Speranza et al., 2004). In order to test the reliability of the RR welded pyroclastic age, we re-assessed the paleomagnetic direction provided for the RR lava flow provided by Arrighi et al. (2006) using the updated SCHA.DIF.4K PSV model from Pavón-Carrasco et al. (2021), which changes to date to AD 1183-1274 (Table 3). This younger date is consistent with that of the RR lava flow (AD 1243-1304).

5. Distal rhyolitic tephra layers on Stromboli and Vulcano islands

White rhyolitic ash layers apparently sourced from Lipari and within the stratigraphic window of this study are recognized on the islands of Stromboli and Vulcano (Fig. 8). These were collected for this study and analyzed for correlation. Although another tephra layer in this time interval was identified above palaeo-detrital deposits containing late Roman age artifacts on Panarea island, and correlated to the MP eruption by Romano (1973), it is no longer exposed and could not been analysed for this study.

On Stromboli, a white ash layer occurs at different sites on the north-eastern sector of the island (40 km NE from Lipari), and it is found directly below the scoria deposits that represent the succession from the onset of the present-day persistent Strombolian activity (Rosi et al., 2000; 2013). The sample analyzed here belongs to a newly discovered outcrop at ~400 m a.s.l. (Fig. 8; 38.795476°N, 15.225255°E). The ash layer shows a variable thickness in the range of 2-5 cm, with a basal, coarser-grained (Mdϕ=1.56), poorly sorted ($\sigma\phi$=2.21) bed and an upper, finer-grained (Mdϕ=3.02), moderately sorted ($\sigma\phi$=1.91) bed. Juvenile pumice account for 70 wt.% of the sample, with a lithic component represented by dark scoria and lavas typical of Stromboli that are possibly introduced into the bed by local wind reworking. When only the juvenile fraction is considered, highly-vesicular pumice with spherical or tubular vesicles represent 98 wt.% of the sample, with dense blocky clasts accounting for the other 2 wt.% (Fig. 9a, b). Major and trace element compositions of the juvenile glass are homogeneous rhyolites with 75.0 ± 0.2 wt.% SiO_2 and 9.0 ± 0.2 wt.%, Na_2O+K_2O (*n=25*), entirely consistent with all the four Lipari eruption deposits investigated here (Fig. 9e-g; Table 2). The average analytical total for these distal glasses is 97.2 ± 1.3 wt.% (1 s.d.), potentially indicating significant H_2O content. Trace elements contents of these rhyolitic glasses show significant heterogeneity with 44.3-55.9 ppm Th, 158-186 ppm Zr, 54.8-66.6 ppm La and 105-129 ppm Ce.

On Vulcano, a white ash layer sourced from Lipari has long been recognized interfingered with some of the products of La Fossa cone (Keller, 1980; Gurioli et al., 2012, De Astis et al., 2013; Di Traglia et al., 2013, Rosi et al., 2018). Specifically, along the flanks of La Fossa cone the ash layer is interlayered within the deposits known as ‘Commenda Breccia‘(Caruggi Formation, ca_1 member; De Astis et al., 2013), recently dated at AD 1250 (Gurioli et al., 2012; Di Traglia et al., 2013; Rosi et al., 2018). An ash layer is also exposed on top of the Vulcanello lava platform interfingered within brownish ash correlated to the ‘Commenda Breccia‘, and thus shares the same stratigraphic position as the sample at La Fossa. The sample analyzed here is related to the ash layer that is exposed on Vulcanello (Fig. 8; 38.425371°N, 14.954087°E), which is ~10 cm

thick and consists of four normal-graded beds (Mdϕ range 1.5-2.5) characterized by an increase of obsidian content from base to top. The componentry analysis carried out on the fraction >500 μm indicates that, on average, the juvenile fraction mostly consists of dense to microvesicular, blocky juvenile clasts and obsidians (59 wt.%) with a subordinate amount of vesicular pumice grains (41 wt.%) (Fig. 9b, d). Obsidian chips are particularly abundant (up to 20 wt.%). Glass compositions of this ash layer are homogeneous rhyolites at a major element level (74.9 ± 0.2 wt.% SiO_2; 9.1 ± 0.2 wt.% $Na_2O + K_2O$ [*n=29*]) (Table 2), and the average analytical total for these glasses is 99.9 ± 0.6 wt.% (1 s.d.) indicating relatively low H_2O contents. The trace element contents are equally very homogeneous (55.9 ± 0.9 ppm Th, 187 ± 3 ppm Zr, 66.6 ± 1.0 ppm La and 128 ± 2 ppm Ce (Fig. 9e-g).

6. Discussion

6.1 Chronology, dispersal and evolution of the eruptive activity

The studied lava flows and pyroclastic deposits of MP, FV, RR and LA resulted from four distinct eruptive events in the last 1500 years, which partially overlapped in time and space. Lithostratigraphic and sedimentological analysis, combined with new radiocarbon and paleomagnetic dates, revisited historical reports, along with geochemical and textural characterization, allow us to propose an updated chronostratigraphic framework for the most recent eruptive history of Lipari (Fig. 10). This reconciles the contradictory chronological attributions in the literature and sheds new light on correlations with distal tephra layers. In particular, we suggest that the MP eruption was the earliest, and the FV, RR and LA eruptions were almost contemporaneous and occurred c. 500 years later. The N-S aligned faults played a major role in controlling the vent locations of the most recent eruptive activity on the island. The different vents and their eruptions are hereafter discussed (starting from the oldest) integrating the different datasets in order to derive chronology, areal dispersal and potential distal correlations.

6.1.1. Monte Pilato

The MP pyroclastic succession is considered the result of a single, relatively continuous explosive eruption based on the fairly homogeneous lithostratigraphic features and absence of internal erosional unconformities. The eruption had a quasi-sustained eruptive regime with significant intensity, and the deposits constructed a 150 m-high pumice cone open to the NE formed mostly from fallout and pyroclastic density current deposits (hereafter PDCs; Dellino and La Volpe, 1995; Forni et al., 2013). The MP activity is the result of a partially collapsing eruption column that produced alternating fallout layers of well-sorted pumice lapilli and poorly-sorted, massive to plane-parallel stratified, ash-supported lapilli beds deposited from PDC activity (in agreement with Dellino and La Volpe, 1995). The eruption evolved through time in a pulsatory eruptive regime with variable energy as shown by the denser stratification of deposits in the upper portion of the succession, with deposits mostly from PDCs and smaller amounts of fallout layers. The coarser (>1 mm) fraction of the 16 samples analysed here are representative of the whole sequence, and document a prevailing highly vesicular juvenile component whose density slightly increases towards the top of the sequence. The eruption was fed by a broadly compositionally homogeneous magma batch since no significant differences in major element compositions have been found among the corresponding products. However, it is important to note that at a trace element level most MP glasses, at different stratigraphic heights, display a substantial compositional variability, while a limited number of samples show a narrow compositional range, indicating no clear relationship between glass composition and stratigraphic height or juvenile texture.

Based on the volume of the outcropping products, the MP eruption represents by far the largest intensity and magnitude eruption on Lipari in the last 1500 years. However, while the thickness of the MP tephra rapidly decreases away from the cone, deposit architecture suggests that most of the deposition occurred towards the northern sector of the island and a substantive portion of

the deposits were possibly emplaced at sea. These observations, linked to the findings of MP rhyolitic tephra (and cryptotephra) within the Marsili basin, and other Tyrrhenian Sea cores (also see Section 6.2), suggest that the eruption is likely to have produced and dispersed a large amount of fine ash with a preferred distribution to the NE that mirrors the main dispersal of the unit in proximal areas.

A shifting to effusive activity likely occurred during the latest phases of the MP eruption as indicated by the increased amount of fresh obsidian fragments towards the top of the tephra sequence and the presence of remnants of an obsidian-rich lava flow that was recognized along the rim of the crater by Forni et al. (2013). Unfortunately, the current state of the outcrop did not allow us to further confirm this observation.

The age of MP eruption is well constrained by the ^{14}C date of AD 780 (AD 675-880) obtained for short-lived, carbonized plant material embedded within the base of the tephra unit (Keller, 2002), which is fully comparable to another radiocarbon age of AD 780-785 previously presented by Keller (1970). This age attribution is in turn consistent with the findings of MP deposits above Greek-Roman ruins dated up to 4–5th centuries AD on Lipari (Keller, 1970), and also with the recognition of a MP distal ash layer above Late Antique Butrint (from late 4th to late 6th century AD) archeological excavations in Albania (Bescoby et al., 2008), although the latter does not provide independent dating and instead uses the tephra layer as a chronological indicator. The age of AD 780 for the MP eruption is further supported by the historical report of the monk Gregorius who in AD 787 described an ongoing eruptive activity on Lipari (Cozza-Luzi, 1890). Moreover, Manni et al. (2018) suggested that the major, long-lasting demographic crisis that occurred on Lipari between the 6th and 11th centuries may have been associated with the peak in eruptive activity of MP. Bernabò Brea (1978; 1989), reported by Cortese et al. (1986), assumed that the explosive eruption described by the bishop Willibald in AD 729 corresponded to the MP eruption, but a careful revision of this chronicle puts this attribution in great doubt, highlighting instead a more probable link with an eruption that occurred on the cone

of La Fossa on volcano. Finally, the legend of Saint Calogero reported by Pichler (1980) apparently describes eruptive activity on Lipari in AD 524-562, but we consider this report unreliable because not clearly indicative of eruptive activity of Mount Pilato on Lipari.

6.1.2. Forgia Vecchia

The FV eruption occurred from a vent around the village of Pirrera. The initial phase of the eruption was explosive, and it was followed by the emission of an obsidian lava flow. A series of explosive pulses from a recurrently collapsing eruption column, which produced fallout pumice lapilli beds, alternated with PDC activity. During the late stages, the explosive activity became more pulsatory and impulsive, with a significant increase of ballistic fallout of fresh obsidian blocks and breadcrust bombs. The lack of internal erosional unconformities suggests that no significative pauses occurred during the explosive activity. The FV deposits built a low-profile tephra ring, which rapidly thins away from the source. The activity ended with the emplacement of an obsidian lava flow that overflowed the eastern rim of the crater and flowed along the pre-existing slope. No subsequent explosive activity is recorded after the effusive phase. Patches of fine-grained, altered to oxidized whitish pyroclastic material recognized above the lava flow are instead related to a different eruption (see Section 6.1.3).

The timing of FV eruption has been controversial, with contrasting absolute and stratigraphic age attributions in the literature (Bigazzi and Bonadonna, 1973; Cortese et al., 1986; Forni et al., 2013). Here we constrain the age of the eruption by combining radiocarbon and paleomagnetic dates. A radiocarbon age of AD 1160-1260 for carbonized material embedded in the upper part of the palaeosol below the FV tephra constrains the onset of the eruption, while the effusive phase is constrained via paleomagnetism to AD 1242-1306. This age is about 900 years younger than the fission-track age of 1.6 ka (AD ~400) by Bigazzi and Bonadonna (1973). This means that the FV eruption occurred after a pause in eruptive activity of c. 500 yrs following the MP eruption. A younger age for FV relative to MP had already been suggested by Forni et al. (2013),

whilst the new age determinations allow us to definitively reject the hypothesis of Cortese et al. (1986) that the FV and MP eruptions were contemporaneous. Eruptive activity in the area of FV is not clearly described in historical reports, an exception is a chronicle of eruptive activity in Lipari in AD 1265 ("*Chronicon aliud breve Pisanum"* cited in Bernabò Brea, 1979), which suggests the likely source of activity was in the area of Pirrera (Guidoboni E., pers. comm.). This date is largely consistent with the ^{14}C and paleomagnetic age derived here for the FV eruption.

6.1.3. Rocche Rosse

The RR eruption occurred from a vent located in the area of Fossa delle Rocche Rosse, within the more elevated part of the MP crater. The initial explosive phase was characterized by multiple pulses of a recurrently collapsing eruption column that produced PDCs and a number of ash and lapilli fallout beds with a significant ballistic component. The near-vent deposits form a low-profile tephra ring hosted within the older MP crater. Thick beds of welded (dark-coloured) juvenile bombs are recognized within the tephra succession only close to the vent. If compared to the characteristics of the underlying MP deposits, the juvenile fraction >1 mm shows striking differences in terms of proportions of dense vs. vesicular components, with the latter being minor to absent. The final phase of the eruption was effusive with the emission of the renowned obsidian lava flow.

As for the chronology of the RR eruption, we obtained a paleomagnetic date of AD 1243-1304 for the lava flow, which is considered more accurate than the slightly older ages of AD 1329-1417 and AD 1420-1490 obtained for the welded dark pumice. The age of AD 1243-1304 is broadly consistent with the age of AD 1220 proposed by Tanguy et al. (2003) and Arrighi et al. (2006) on the basis of archeomagnetism, and it is our preferred age attribution for RR, being substantially younger than the fission track age of 1.4 ka by Bigazzi and Bonadonna (1973). There are no historical reports of an eruption in the study area in this time interval although, as noted previously, there was a demographic crisis in the study area between the 6^{th} and 11^{th}

centuries (Manni et al., 2018). On the other hand, the chronicle of eruptive activity on Lipari in AD 1265 (Bernabò Brea, 1979), mentioned above for the FV eruption, could also be related to contemporaneous activity from multiple vents in the area of Forgia Vecchia and Rocche Rosse.

Based on the proposed age attributions and stratigraphic correlations, we suggest that the altered and oxidized whitish pyroclastic material recognized above the FV lava flow can be attributed to the RR explosive phase, suggesting a southwards dispersal for the RR fallout products. This tephra bed mantles an irregular, blocky lava surface, not yet modified by erosion. Moreover, the high degree of tephra alteration and hardening may be attributed to high-temperature fluids circulation, which indicates that the FV lava flow was still hot when the RR tephra deposited and confirms that the two eruptions were near-contemporaneous.

6.1.4. Lami

The LA tephra is considered the product of a small-magnitude eruption from a lateral vent along the southern flank of the MP cone. The eruption showed repeated eruptive pulses that produced discrete lapilli fallout beds, ballistic bombs and blocks, and minor dilute PDCs, which are all characterized by a limited thickness around the vent. The LA tephra built a low-profile cone along the lower elevated part of the southern flank of the MP cone (Forni et al., 2013). During the latest phases of the eruption, low-fountaining produced a layer of densely welded, highly vesicular pumice recognized at top of the succession. The abundance of ballistic clasts that are up to 50 cm in diameter (breadcrust bombs, lithics of rhyolite lava and abundant fresh obsidian blocks) are indicative of proximality to the vent (Pichler, 1976; Cortese et al., 1986; Dellino, 1991; Lucchi et al., 2010; Forni et al., 2013). This observation, combined with a distinctive componentry, allows us to reject the alternative hypothesis that the LA tephra is a part of the MP pyroclastic succession that was suggested by Davì et al. (2011).

We paleomagnetically dated the LA eruption to AD 1253-1316, which is consistent with the fission track age of 700 years BP (AD 1250) by Bigazzi et al. (2003). The LA activity is thus

almost contemporaneous with the RR eruption, as previously suggested by Forni et al. (2013) based on stratigraphic features. The occurrence of some ash beds interlayered within the LA succession that have the distinctive weakly vesicular pumice components of the RR tephra is further evidence for contemporaneous activity from the different vents. We did not recognize any ash layers with the grain-size and componentry of the MP tephra within the LA succession, which has led us to exclude the hypothesis of Cortese et al. (1986) that the LA and MP eruptions were contemporaneous, as also confirmed by our new age attributions.

6.2. Proximal-medial-distal correlations of Lipari-sourced rhyolitic tephra

The new chrono-stratigraphic framework for the MP, FV, RR and LA eruptions, combined with lithological and textural characterization and geochemical analysis of the glass, have important implications for the use of the corresponding tephra layers as chronostratigraphic markers in the Aeolian Islands region and across the southern Mediterranean area. Lipari-sourced rhyolitic tephra and cryptotephra layers have been recognized subaerially on the Aeolian Islands (see Keller, 1980; Rosi et al., 2000; Lucchi et al., 2013d; Albert et al., 2017; Rosi et al., 2018) as well as in marine sediment sequences of the southern Tyrrhenian (Paterne et al., 1988; Di Roberto et al., 2008; Albert et al., 2012, 2017) and Northern Ionian (Caron et al., 2012; Menke et al., 2018; Di Donato et al., 2019; Insinga et al., 2020) seas. Based on their rhyolitic composition, aphyric texture and stratigraphic position above the widespread Vallone del Gabellotto marker bed, these distal tephra layers have been generally correlated to the MP eruption, which was considered that with the largest magnitude and dispersal. However, correlations of these distal tephra layers to the individual eruption deposits described in detail in this paper have not previously been attempted.

Here we utilize newly reported glass geochemical analyses of the rhyolitic ash layers on Stromboli and Vulcano, along with a re-appraisal of deposits found in the area of the Monte San Angelo on Lipari (Albert et al., 2017), to validate proximal-medial-distal correlations. The

largely overlapping major and trace element glass chemistries of the MP, FV, RR and LA volcanic glasses mean that a chemical approach alone cannot be used to determine the individual source eruption of a distal rhyolitic tephra. However, there are some subtle diagnostic features of the different proximal eruption deposits. MP erupted glasses consistently have the lowest major element analytical totals, probably indicating higher H_2O contents in these young, fresh deposits, although this feature is less suitable when dealing with fine distal marine tephra samples. More importantly, MP glasses display a larger degree of trace element variability with respect to the younger FV, RR and LA eruption deposits (Fig. 3). Unfortunately, trace element compositions of distal marine Lipari-sourced samples are not extensively reported in the literature. As a consequence of the limited discrimination potential of volcanic glass geochemical features, correlations between the different eruption deposits also take into account the texture of juvenile clasts carried out on comparable grain-size fractions, combined with the reconstructed areal distribution of the deposits and local stratigraphy in the medial-distal locations. We do not take into account the variability of vesicularity/density highlighted for MP by Dellino and La Volpe (1995) in the finest <63 μm ash fractions.

Albert et al. (2012, 2017) reported medial fall deposits of MP on top of Monte San Angelo (Central Lipari), based on their apparent stratigraphic position upon a paleosol formed above the Vallone del Gabellotto products, and used their geochemical signature as the reference for correlation with distal rhyolitic tephra deposits in the historical timeframe. Our new analysis of the proximal MP succession raises uncertainty over the attribution of these Monte San Angelo deposits to MP. Trace element glass compositions from the deposits above the Monte San Angelo unit (Albert et al., 2017) are distinct from those of the eruption deposits of the last 1,500 years that are documented in this paper and the near-vent MP succession. Specifically, using the Th vs. LREE bi-plots (La, Ce) adopted to discriminate the successive eruptions on Lipari by Albert et al. (2017), it appears that the deposits on Monte San Angelo are offset to lower LREE content and are instead in better agreement with the underlying Vallone del Gabellotto eruption

unit, or at least reside on a similar evolutionary trend (Fig. 9). However, glasses in the upper portion of the deposits on Monte San Angelo extend to higher incompatible trace element contents (including Th, U, Nb) relative to the Vallone del Gabellotto products, and in this sense are more similar to those of MP and other historical eruption deposits. Based on these conflicting chemical features, we tentatively suggest that the deposits on Monte San Angelo are related to another eruption chrono-stratigraphically between Vallone del Gabellotto and MP, which we did not observe in the proximal record. Indeed, distal ash fall records already suggest the Early-Holocene eruptive activity of Lipari, particularly associated with the Vallone del Gabellotto, is not fully captured by current proximal sequences as there are at least two stratigraphically separated ash fall events in this time-interval reported in different marine cores (Siani et al., 2004; Crocitti et al., 2019). Furthermore, sediment cores from the Ionian Sea, Gulf of Taranto, suggest at least three Lipari-sourced ash fall events in the Late-Holocene, with one predating the MP eruption (Di Donato et al., 2019). Given the uncertainty surrounding the origin of the deposits recognized on Monte San Angelo by Albert et al. (2017), we recommend adopting the glass chemistry of the near-vent MP deposits presented here for future proximal-medial-distal correlations.

The distal rhyolitic tephra layer recognized in several outcrops on Stromboli island is here correlated to the MP eruption based on the occurrence of distinctive (dominant) highly vesicular pumice clasts. This correlation is also supported by glass geochemistry. The low (avg. ~97 wt.%) major element analytical totals for this tephra layer suggest it is consistent with those of the MP (Table 2). Most importantly, the trace element contents of the tephra layer on Stromboli show a greater heterogeneity than the FV, RR and LA eruption deposits - a distinctive feature of the MP eruption products (Fig. 9). Moreover, the distal tephra layer is recognized immediately below the deposits related to the present-day activity of Stromboli that are independently dated to the 7^{th}-8^{th} century using ^{14}C (Rosi et al., 2000), which is in good agreement with the age of the MP eruption. Given that the main dispersal of the MP tephra observed in proximal areas is towards

NE, a correlation of the tephra on Stromboli with the MP eruption is also consistent with the NE location of Stromboli with respect to Lipari. The area of fallout dispersal is crucial as most of the MP-sourced rhyolitic tephra (and cryptotephra) layers recovered from marine sediments occur to the NE and E of the source area. A rhyolitic ash layer was also found on top of a marine sediment core in the Marsili Basin (TIR2000-C01; Di Roberto et al., 2008; Albert et al., 2012), c. 75 km to the N of Lipari. Although glass compositions are not conclusive, we suggest that this marine tephra layer is related to the MP eruption due to the distinctive presence of dominant highly vesicular glass shards with tubular vesicles which characterize MP pyroclastic deposits. Another rhyolitic ash layer was identified in a sedimentary sequence in Albania, c. 600 km NE from Lipari (Bescoby et al., 2008), and correlated to MP eruption, although no independent age is provided. The identification of the MP in marine cores through detailed chemical fingerprinting (Di Roberto et al., 2008; Albert et al., 2017) and the absolute age determinations (Paterne et al., 1988) substantially extend the dispersal of MP to the N, suggesting that much of the Tyrrhenian area could have been covered by tephra fallout during the MP eruption. By these means, the MP eruption is affirmed as the highest magnitude/intensity eruption during the last 1500 years of activity on Lipari.

The rhyolitic Lipari-sourced ash layer documented on Vulcano in different sites along the flanks of La Fossa cone and Vulcanello has been long attributed to the MP eruption (Keller, 1980; De Astis et al., 2013), based on the idea that this was the only one eruption able to disperse fine ash over large areas. However, a recent paleomagnetic age of AD 1250 for the ‘Commenda Breccia‘ unit into which the ash layer is interfingered (Gurioli et al., 2012; Di Traglia et al., 2013; Rosi et al., 2018) makes an attribution to the MP eruption unlikely, instead suggesting a possible correlation with the RR eruption. We note that the homogeneous rhyolitic glass compositions of the different eruption deposits in the investigated time span are not helpful in supporting any specific correlations, because the distal ash layer fits generically with the compositional field involving all the studied proximal units on Lipari (Fig. 9). However, given a larger degree of

heterogeneity at a trace element level of the MP tephra it seems unlikely that the Vulcano ash bed can be attributed to this eruption. Furthermore, the textural analysis indicates the distal ash layer on Vulcano mostly consists of blocky dense to microvesicular juvenile clasts and obsidians, which is feature of the RR eruption deposits and not consistent with those of the MP eruption (Fig. 9). Considering the proximal MP deposits show an increase in obsidian chips and a slight decrease in vesicularity towards the top of the sequence, it could be argued that the Vulcano rhyolitic ash could result from a final phase of MP eruption. This is not supported by the overall characteristics of the ash on Vulcano as 80% of the clasts are high-density and blocky, which is not observed even in the final phases of proximal MP eruption deposit. For the same reason, the highly vesicular LA and FV eruption deposits are not proximal counterparts of the ash layer on Vulcano. A correlation between the ash layer on Vulcano, located south of Lipari, with the RR eruption is consistent with the southwards dispersal of the eruption, confirmed by the occurrence of its altered tephra above the FV lava flow, and that the older MP eruption deposits are mostly dispersed to the NE. Although our data are not fully conclusive, a correlation of the tephra layer on Vulcano with the RR eruption is most likely based on our current knowledge.

Interestingly, rhyolitic tephra layers were identified along an eastern axis from Lipari, i.e. in the Gulf of Taranto and in the Ionian Sea (Di Donato et al., 2019; Caron et al., 2012). Given the AD 1321-1349 date for the tephra , Caron et al. (2012) attributed it to a generic MP eruption. Menke et al. (2018) also identified a rhyolitic tephra layer which they attributed to MP based on ^{14}C age determinations and an age model based on the sedimentation rate in that area, while leaving open the possibility of a younger age (i.e. 13^{th} century). The attribution to eruptive events younger than MP was however discarded due to their reduced volume and intensity compared to MP. These tephra layers cannot be univocally attributed to MP or to other more recent eruptions on Lipari because the existing geochemical correlations are not conclusive and some of the independent age constraints can be debated. However, it is likely that there was (at least) one

eruption younger than MP in the 13th century that dispersed ash to the E forming ash layers in the Mediterranean. Considering that the ash layers in the Ionian Sea are all composed of vesicular glass fragments, we propose that the FV eruption is the potential proximal equivalent of these distal layers (RR has a dominant dense juvenile component and Southwards dispersal), even if the LA eruption could have also produced some widely dispersed ash to the east. It is notable that the FV eruption was probably not considered in the previous papers because its age attribution was ambiguous. A chemical and chronological re-appraisal, where trace elements are used to identify MP candidates, and purely independent age models for the respective marine cores (Lipari historical eruption ages are excluded), is needed to validate these proximal-to-distal correlations.

7. Conclusive remarks

In this paper we have adopted a multidisciplinary approach, and combined volcanological and stratigraphic analyses with paleomagnetic and ^{14}C dates of lava flows and tephra units in the NE sector of Lipari island with a re-evaluation of historical reports, which provide a new chrono-stratigraphic framework for the most recent rhyolitic eruptive cycle in the last 1500 years. The earliest eruption in the investigated time span was that of Monte Pilato during the late 8th century, which led to the formation of a pumice cone and produced a substantial tephra dispersal extending towards the NE. This eruption was the most energetic and capable of dispersing volcanic ash across a large area, as validated by correlations with distal tephra layers on Stromboli island and in marine sediment sequences in the southern Tyrrhenian Sea. A significantly younger age (c. 500 yrs after the Monte Pilato eruption) is proposed here for the Forgia Vecchia eruption, derived from consistent paleomagnetic and radiocarbon ages and re-appraisal of historical reports. Forgia Vecchia is thought to have produced a tephra dispersal that extended towards the Ionian Sea and the Gulf of Taranto.

Stratigraphic analysis and paleomagnetic ages for Rocche Rosse (AD 1243-1304) and Lami (AD

1253-1316) indicate that the two eruptions were probably contemporaneous with the activation of N-S-aligned different vents, and these occurred shortly after the Forgia Vecchia eruption.

Accurate age assessment of the different eruptions, combined with textural and geochemical characteristics of the glass fragments and information on the dispersal of each tephra have offered further information on the tephrochronological use of the most recent Lipari-sourced rhyolitic ash beds and cryptotephra layers in continental and marine settings. While many distal ash layers found in subaerial settings (Stromboli) and marine cores may be confidently attributed to the Monte Pilato eruption, our reconstruction indicates that the younger eruptions from Lipari during the 13th century may have produced further tephra occurrences in subaerial areas (Rocche Rosse on Vulcano), and in marine cores (Forgia Vecchia in the Ionian sea) with the latter requiring further investigations. Based on the collected data, we finally remark that all the studied historical rhyolitic eruptions show almost identical glass chemistries, implying that it is difficult to use a geochemical fingerprint alone to establish precise source correlations for distal tephra layers, and consequently, detailed chrono-stratigraphy, combined with information on physical features of tephra and dispersal characteristics also need to be considered.

CRediT author statement

M. Pistolesi, M. Rosi, F. Speranza, F. Lucchi, C. Tranne: Conceptualization. **M. Pistolesi, M. Rosi, F. Speranza, F. Lucchi, C. Tranne, A.B Malaguti**: Investigation. **M. Pistolesi, M. Rosi, F. Speranza, A.B. Malaguti, P.G. Albert, V. Smith, A. Di Roberto, E. Billotta**: Data curation. **M. Pistolesi, A.B Malaguti**: Writing-Original draft preparation. **M. Pistolesi, M. Rosi, F. Speranza, F. Lucchi, C. Tranne, P.G. Albert, V. Smith**: Writing- Reviewing and Editing.

Declaration of interests

The authors declare that they have no known competing financial interests or personal relationships that could have appeared to influence the work reported in this paper.

The authors declare the following financial interests/personal relationships which may be considered as potential competing interests:

References

Albert, P.G., Tomlinson, E.L., Smith, V.C., Di Roberto, A., Todman, A., Rosi, M., Marani, M., Muller, W., Menzies, M.A., 2012. Marine-continental tephra correlations: volcanic glass geochemistry from the Marsili Basin and the Aeolian Islands, Southern Tyrrhenian Sea, Italy. J Volcanol Geotherm Res 229–230, 74–94.

Albert, P.G., Tomlinson, E.L., Smith, V.C., Di Traglia, F., Pistolesi, M., Morris, A., Donato, P., De Rosa, R., Sulpizio, R., Keller, J., Rosi, M., 2017. Glass geochemistry of pyroclastic deposits from the Aeolian Islands in the last 50 ka: a proximal database for tephrochronology. J Volcanol Geotherm Res 336:81–107,

Arrighi, S., Tanguy, J.C., Rosi, M., 2006. Eruptions of the last 2200 years at Vulcano and Vulcanello (Aeolian Islands, Italy) dated by high-accuracy archeomagnetism. Phys. Earth Planet. Inter. 159, 225–233.

Barberi, F., Gandino, A., Gioncada, A., La Torre, P., Sbrana, A., Zenucchini, C., 1994. The deep structure of the Eolian arc (Filicudi-Panarea-Vulcano sector) in light of gravity, magnetic and volcanological data. J Volcanol Geotherm Res 61:189–206.

Bernabò Brea L., 1978. Lipari, Vulcano, l'inferno e San Bartolomeo. Le Isole Eolie dal tardo antico ai Normanni. Archivio Storico Siracusano, pp. 48-55.

Bernabò Brea L., 1989. Le Isole Eolie dal tardo antico ai Normanni. Università degli studi di Bologna, Istituto di antichità ravennati e bizantine, Mario Lapucci Edizioni del Girasole, pp. 36-45.

Bescoby, D., Barclay, J., Andrews, J., 2008. Saints and sinners: a tephrochronology for Late Antique landscape change in Epirus from the eruptive history of Lipari, Aeolian Islands. J. Archaeol. Sci. 35(9), 2574-2579.

Bigazzi, G., Bonadonna, F.P., 1973. Fission track dating of the obsidian of Lipari Island (Italy). Nature 242:322–323.

Bigazzi, G., Coltelli, M., Norelli, P., 2003. Nuove età delle ossidiane di Lipari determinate con il metodo delle tracce di fissione. GeoItalia, 4th Forum FIST, Bellaria, 16–18 September, Abstract Volume 1: 444–446.

Billi, A., Barberi, G., Faccenna, C., Neri, G., Pepe, F., Sulli, A., 2006. Tectonics and seismicity of the Tindary Fault System, southern Italy: Crustal deformations at the transition between ongoing contractional and extensional domains located above the edge of a subducting slab. Tectonics 25.

Branca, S., D'Ajello Caracciolo, F., Malaguti, A.B., Speranza, F., 2019. Constraining age and volume of lava flow invasions of the Alcantara valley, Etna volcano (Italy). New insights from paleomagnetic dating and 3D magnetic modeling. J. Volcanol. Geotherm. Res. 374, 13–25.

Brock, F., Higham, T., Ditchfield, P., Ramsey, C.B., 2010. Current pretreatment methods for AMS radiocarbon dating at the Oxford Radiocarbon Accelerator Unit (ORAU). Radiocarbon, 52(1), 103-112.

Bullock, L.A., Gertisser, R., O'driscoll, B., 2018. Emplacement of the Rocche Rosse rhyolite lava flow (Lipari, Aeolian Islands). Bull Volcanol, 80(5), 1-19.

Caron, B., Siani, G., Sulpizio, R., Zanchetta, G., Paterne, M., Santacroce, R., Tema, E., Zanella, E., 2012. Late Pleistocene to Holocene tephrostratigraphic record from the Northern Ionian Sea. Mar. Geol. 311–314, 41–51.

Cas, R.A.F., Wright, J.V., 1987. Volcanic successions. Modern and ancient. Allen and Unwin, London, p 528.

Cortese, M., Frazzetta, G., La Volpe, L., 1986. Volcanic history of Lipari (Aeolian Islands, Italy) during the last 10,000 years. J Volcanol Geotherm Res 27:117–133.

Cozza-Luzi, G., 1890. Le eruzioni di Lipari e del Vesuvio nell'anno 787. Tipografia pontificia di San Giuseppe, Milano.

Crisci, G.M., De Rosa, R., Esperanca, S., Mazzuoli, R., Sonnino, M., 1991. Temporal evolution of a 3 component system-the island of Lipari (Aeolian Arc, southern Italy). Bull Volcanol 53(3):207–221.

Crocitti, M., Sulpizio, R., Insinga, D.D., De Rosa, R., Donato, P., Iorio, M., Zanchetta, G., Barca, D., Lubritto, C., 2019. On ash dispersal from moderately explosive volcanic eruptions: Examples from Holocene and Late Pleistocene eruptions of Italian volcanoes. J Volcanol Geotherm Res 385:198–221.

Davì, M., De Rosa, R., Barca, D., 2009. A LA-ICP-MS study of minerals in the Rocche Rosse magmatic enclaves: evidence of a mafic input triggering the latest silicic eruption of Lipari Island (Aeolian Arc, Italy). J Volcanol Geotherm Res 182:45–56.

Davì, M., De Rosa, R., Donato, P., Sulpizio, R., 2011. The Lami pyroclastic succession (Lipari, Aeolian Islands): a clue for unravelling the eruptive dynamics of the Monte Pilato rhyolitic pumice cone. J Volcanol Geotherm Res 201:285–300.

De Astis, G., Lucchi, F., Dellino, P., La Volpe, L., Tranne, C.A., Frezzotti, M.L., Peccerillo, A., 2013. Geology, volcanic history and petrology of Vulcano (central Aeolian archipelago). Geol Soc Lond Mem 37: 281–349.

De Beaulieu, J.L., Brugiapaglia, E., Joannin, S., Guiter, F., Zanchetta, G., Wulf, S., Peyron, O., Bernardo, L., Didier, J., Stock, A., Rius, D., Magny, M., 2017. Lateglacial-Holocene abrupt vegetation changes at Lago Trifoglietti in Calabria, Southern Italy: The setting of ecosystems in a refugial zone. Quaternary Science Reviews, 158, 44-57.

De Fiore O., 1922. Vulcano. Cozzolino, Napoli, pp. 164-165.

De Rosa, R., Donato, P., Gioncada, A., Masetti, M., Santacroce, R. 2003. The Mt. Guardia eruption (Lipari Aeolian Islands): an example of a reversely zoned magma mixing sequence. Bull Volcanol 65:530–543.

Dellino, P., 1991. Metodi quantitativi applicati allo studio dei depositi piroclastici. Il caso di M. Pilato – Rocche Rosse. Unpublished, PhD thesis, University of Bari, Italy.

Dellino, P., La Volpe, L., 1995. Fragmentation versus transportation mechanisms in the pyroclastic sequence of Monte Pilato–Rocche Rosse (Lipari, Italy). J Volcanol Geotherm Res 64:211–231.

Di Chiara, A., Speranza, F., Porreca, M., 2012. Paleomagnetic secular variation at the Azores during the last 3 ka. Journal of Geophysical Research: Solid Earth, 117(B7).

Di Chiara, A., Speranza, F., Porreca, M., Pimentel, A., D'Ajello Caracciolo, F., Pacheco, J., 2014. Constraining chronology and time-space evolution of Holocene volcanic activity on the Capelo Peninsula (Faial Island, Azores): The paleomagnetic contribution. Bulletin, 126(9-10), 1164-1180.

Di Donato, V., Insinga, D. D., Iorio, M., Molisso, F., Rumolo, P., Cardines, C., Passaro, S., 2019. The palaeoclimatic and palaeoceanographic history of the Gulf of Taranto (Mediterranean Sea) in the last 15 ky. Global and Planetary Change, 172, 278-297.

Di Martino, C., Frezzotti, M.L., Palmeri, R., Lucchi, F., Peccerillo, A., Tranne, C.A., Diamond, L.W., 2010. Magma storage and ascent at Lipari Island (Aeolian archipelago, Southern Italy) at 223-81 ka: the role of crustal processes and tectonic influence. Bull Volcanol. doi: 10.1007/s00445-010-0383-6.

Di Roberto, A., Rosi, M., Bertagnini, A., Marani, M.P., Gamberi, F., Del Principe, A., 2008. Deep water gravity core from the Marsili Basin (Tyrrhenian Sea) records Pleistocene-Holocenic explosive events and instabilities of the Aeolian Island Archipelago, (Italy). J. Volcanol. Geotherm. Res. 177 (1), 133–144.

Di Roberto, A., Smedile, A., Del Carlo, P., De Martini, P. M., Iorio, M., Petrelli, M., Pantosti, D., Pinzi, S., Todrani, A., 2018. Tephra and cryptotephra in a ~60,000-year-old lacustrine sequence from the fucino basin: New insights into the major explosive events in Italy. Bull Volcanol, 80(3), 1-23.

Di Traglia, F., Pistolesi, M., Rosi, M., Bonadonna, C., Fusillo, R., Roverato, M., 2013. Growth and erosion: volcanic geology and morphological evolution during the last 1000 years of La Fossa (island of Vulcano, southern Italy). Geomorph 194:94–107.

Fisher, R.A., 1953 Dispersion on a sphere. Phil. Trans. R. Soc. A 217:195–305.

Forni, F., Lucchi, F., Peccerillo, A., Tranne, C.A., Rossi, P.L., Frezzotti, M.L., 2013. Stratigraphy and geological evolution of the Lipari volcanic complex (central Aeolian archipelago). Geol Soc London Mem 37: 213–279.

Forni, F., Ellis, B.S., Bachmann, O., Lucchi, F., Tranne, C.A., Agostini, S., Dallai, L., 2015. Erupted cumulate fragments in rhyolites from Lipari (Aeolian Islands). Contrib Mineral Petrol 170:1–18.

Fusillo, R., Di Traglia, F., Gioncada, A., Pistolesi, M., Wallace, P.J., Rosi, M., 2015 Deciphering post-caldera volcanism: insight into the Vulcanello (island of Vulcano, southern Italy) eruptive activity based on geological and petrological constraints. Bull Volcanol 77:76.

Gillot, P.Y., 1987. Histoire volcanique des Iles Eoliennes: arc insulaire ou complexe orogenique annulaire?. Documents et travaux de l'Institut géologique Albert de Lapparent, (11), 35-42.

Gioncada, A., Mazzuoli, R., Bisson, M., Pareschi, M.T., 2003. Petrology of volcanic products younger than 42 ka on the Lipari–Vulcano complex (Aeolian Islands, Italy): an example of volcanism controlled by tectonics. J Volcanol Geotherm Res 122:191–220.

Greve, A., Turner, G.M., 2017. New and revised palaeomagnetic secular variation records from post-glacial volcanic materials in New Zealand. Physics of the Earth and Planetary Interiors, 269, 1-17.

Gurioli, L., Zanella, E., Gioncada, A., Sbrana, A., 2012. The historic magmatic-hydrothermal eruption of the Breccia di Commenda, Vulcano, Italy. Bull Volcanol 74(5):1235–1254.

Inman, D.L., 1952. Measures for describing the size distribution of sediments. J Sediment Petrol 22:125–145.

Insinga, D.D., Petrosino, P., Alberico, I., de Lange, G.J., Lubritto, C., Molisso, F., Sacchi, M., Sulpizio, R., Wu, J., Lirer, F., 2020. The Late Holocene tephra record of the central Mediterranean Sea: Mapping occurrences and new potential isochrons for the 4.4–2.0 ka time interval. Journal of Quaternary Science, 35(1-2), 213-231.

Juárez-Arriaga, E., Böhne,l H., Carrasco-Núñez, G., Mahgoub, A.N., 2018. Paleomagnetism of Holocene lava flows from Los Humeros caldera, eastern Mexico: Discrimination of volcanic eruptions and their age dating. Journal of South American Earth Sciences, 88, 736-748.

Jochum, K.P., Stoll, B., Herwig, K., Willbold, M., Hofmann, A.W., Amini, M., Aaburg, S., Abouchami, W., Hellebrand, E., Mocek, B., Raczek, I., Stracke, A., Alard, O., Bouman, C., Becker, S., Dücking, M., Brätz, H., Klems, R., de Bruin, D., Canil, D., Cornell, D., de Hoog, C.J., Dalpé, C., Danyusheysky, L., Eisenhauer, A., Gao, Y., Snowm J.E., Groschopf, N., Günther, D., Latkoczy, C., Guillong, M., Hauri, E.H., Höfer, H.E., Lahaye, Y., Horz, K., Jacob, D.E., Kasemann, S.A., Kent, A.J.R., Ludwing, T., Zack, T., Mason, P.R.D., Meixner, A., Rosner, M., Misawa, K., Nash, B.P., Pfänder, J., Premo, W.R., Sun, W.D., Tiepolo, M., Vannucci, R., Vennemann, T., Wayene, D., Woodhead, J.D., 2006. MPI-DING reference glasses for in situ microanalysis: New reference values for element concentrations and isotope ratios. Geochemistry, Geophysics, Geosystems, 7(2).

Keller, J., 1970. Datierung der obsidiane und bimstuffe von Lipari. Neues Jahrbuch für Geologie und Paläeontologie, 90-101.

Keller, J., 1980. The Island of Vulcano. Rendiconti della Società Italiana di Mineralogia e Petrologia 36:369–414.

Keller, J., 2002. Lipari's fiery past: dating the Medieval pumice eruption of Monte Pilato. International Conference UNESCO-Regione Siciliana, Lipari, September 29–October 2.

Kirschvink, J.L., 1980. The least-square line and plane and the analysis of paleomagnetic data. Geophys. J. 62: 699–718.

Lanza, R., Zanella, E., 1991. Palaeomagnetic directions (223-1.4 ka) recorded in the volcanites of Lipari, Aeolian Islands. Geophysical journal international, 107(1), 191-196.

Lanzafame, G., Bousquet, J.C., 1997. The Maltese escarpment and its extension from Mt. Etna to Aeolian Islands (Sicily): importance and evolution of a lithosphere discontinuity. Acta Vulcanologica, 9, 113-120.

Le Bas, M.J., Le Maitre, R.W., Streckeisen, A., Zanettin, B., 1986. A chemical classification of volcanic rocks based on the total alkali–silica diagram. J. Petrol. 27, 745–750.

Leonhardt, R., Matzka, J., Nichols, A.R.L., Dingwell, D.B., 2006. Cooling rate correction of paleointensity determination for volcanic glasses by relaxation geospeedometry. Earth and Planetary Science Letters, 243(1-2), 282-292.

Lucchi, F., Tranne, C.A., Calanchi, N., Rossi, P.L., 2007. Late Quaternary deformation history of the volcanic edifice of Panarea, Aeolian Arc, Italy. Bull Volcanol, 69(3), 239-257.

Lucchi, F., Tranne, C.A., Rossi, P.L., 2010. Stratigraphic approach to geological mapping of the late-Quaternary volcanic island of Lipari (Aeolian archipelago, Southern Italy). Stratigraphy and Geology of Volcanic Areas. Geological Society of America, Boulder, Special Papers, 464, 1-32.

Lucchi, F., Gertisser, R., Keller, J., Forni, F., De Astis, G., Tranne, C.A., 2013a. Eruptive history and magmatic evolution of the island of Salina (central Aeolian archipelago). Geol Soc London Mem 37:155– 211.

Lucchi, F., Keller, J., Tranne, C.A., 2013b. Regional stratigraphic correlations across the Aeolian archipelago (southern Italy). Geol Soc London Mem 37:55–81.

Lucchi, F., Tranne, C.A., Forni, F., Rossi, P.L., 2013c. Geological map of the island of Lipari, scale 1:10 000 (Aeolian archipelago). Geol Soc London Mem 37, enclosed DVD.

Lucchi, F., Tranne, C.A., Peccerillo, A., Keller, J., Rossi, P.L., 2013d. Geological history of the Panarea volcanic group (eastern Aeolian archipelago). Geol Soc London Mem 37(1), 351-395.

Manni, M., Coltelli, M., Martinelli, M., Martinelli, M.C., 2018. Volcanic events that have marked the anthropic history of the Aeolian Islands. Annals of Geophysics, 62(1), 08.

Mazzuoli, R., Tortorici, L., Ventura, G., 1995. Oblique rifting in Salina, Lipari and Vulcano islands (Aeolian islands, southern Italy). Terra Nova, 7(4), 444-452.

Menke, V., Kutterolf, S., Sievers, C., Schindlbeck, J.C., Schmiedl, G., 2018. Cryptotephra from Lipari Volcano in the eastern Gulf of Taranto (Italy) as a time marker for paleoclimatic studies. Quaternary Research, 89(2), 520.

Paterne, M., Guichard, F., Labeyrie, J., 1988. Explosive activity of the South Italian volcanoes during the past 80,000 years as determined by marine tephrochronology. J Volcanol Geotherm Res, 34(3-4), 153-172.

Pavón-Carrasco, F.J., Rodríguez-González, J., Osete, M.L., Torta, J.M., 2011. A Matlab tool for archaeomagnetic dating. J. Archaeol. Sci. 38:408–41.

Pavón-Carrasco, F.J., Campuzano, S.A., Rivero-Montero, M., Molina-Cardín, A., Gómez-Paccard, M., Osete, M.L., 2021. SCHA.DIF.4k: 4,000 Years of Paleomagnetic Reconstruction for Europe and Its Application for Dating. Journal of Geophysical Research: Solid Earth, 126(3), e2020JB021237.

Pichler, H., 1976. Carta geologica dell'Isola di Lipari (scala 1: 10,000). Firenze, Litografia Artistica Cartografica.

Pichler, H., 1980. The island of Lipari. Rendiconti della Società Italiana di Mineralogia e Petrologia 36:415–440.

Ramsey, C.B., 2009. Bayesian analysis of radiocarbon dates. Radiocarbon, 51(1), 337-360.

Ramsey, C.B., Higham, T., & Leach, P., 2004. Towards high-precision AMS: progress and limitations. Radiocarbon, 46(1), 17-24.

Reimer, P.J., Austin, W.E., Bard, E., Bayliss, A., Blackwell, P.G., Bronk Ramsey, C., Butzin, M., Cheng, H., Lawrence Edwards, R., Friedrich, M., Grootes, P.M., Guilderson, T.P., Hajdas, I., Heaton, T.J. Hogg, A.G, Hughen, K.A., Kromer, B., Manning, S.W., Muscheler,

R., Palmer, J.G., Pearson, C., van der Plicht, J., Reimer, R.W., Richards, D.A., Marian Scott, E., Southan, J.R., Turney, C.S.M., Wacker, L., Adolphi, F., Büntegen, U., Capano, M., Fahrni, S.M., Fogtmann-Schulz, A., Friedrich, R., Köhler, P., Kudsk, S., Miyake, F., Olden, J., Reinig, F., Sakamoto, M., Sookdeo, A., Talamo, S., 2020. The IntCal20 Northern Hemisphere radiocarbon age calibration curve (0–55 cal kBP). Radiocarbon, 62(4), 725-757.

Risica, G., Speranza, F., Giordano, G., De Astis, G., Lucchi, F., 2019. Palaeomagnetic dating of the Neostromboli succession. J Volcanol Geotherm Res, 371, 229-244.

Risica, G., Di Roberto, A., Speranza, F., Del Carlo, P., Pompilio, M., Meletlidis, S., Rosi, M., 2020. Refining the Holocene eruptive activity at Tenerife (Canary Islands): The contribution of palaeomagnetism. J Volcanol Geotherm Res, 106930.

Romano, R., 1973. Le Isole di Panarea e Basiluzzo. Contributo alla conoscenza geo-vulcanologica e magmatologica delle Isole Eolie: Rivista Mineralogica Siciliana, v. XXIV, no. 139–141: Publ. N. v. 46, p. 3–40.

Rosi, M., Bertagnini, A., Landi. P., 2000. Onset of the persistent activity at Stromboli volcano (Italy). Bull Volcanol 62:294–300.

Rosi, M., Pistolesi, M., Bertagnini, A., Landi, P., Pompilio, M., Di Roberto, A., 2013. Stromboli volcano, Aeolian Islands (Italy): present eruptive activity and hazards. Geol Soc London Mem 37(1), 473-490.

Rosi, M., Di Traglia, F., Pistolesi, M., Esposti Ongaro, T., de' Michieli Vitturi, M., Bonadonna, C., 2018. Dynamics of shallow hydrothermal eruptions: new insights from Vulcano's Breccia di Commenda eruption. Bull Volcanol 80:1–28.

Ruch, J., Vezzoli, L., De Rosa, R., Di Lorenzo, R., Acocella, V., 2016. Magmatic control along a strike-slip volcanic arc: the central Aeolian arc (Italy). Tectonics 35:407–424.

Selva, J., Bonadonna, C., Branca, S., De Astis, G., Gambino, S., Paonita, A., Pistolesi, M., Ricci, T., Sulpizio, R., Tibaldi, A., Ricciardi, A., 2020. Multiple hazards and paths to eruptions: A

review of the volcanic system of Volcano (Aeolian Islands, Italy). Earth-Science Reviews, 103186.

Shields, J.K., Mader, H.M., Caricchi, L., Tuffen, H., Mueller, S., Pistone, M., Baumgartner, L., 2016. Unravelling textural heterogeneity in obsidian: shear-induced outgassing in the Rocche Rosse flow. J Volcanol Geotherm Res, 310, 137-158.

Siani, G., Sulpizio, R., Paterne, M., Sbrana, A., 2004. Tephrostratigraphy study for the last 18,000 14C years in a deep-sea sediment sequence for the South Adriatic. Quaternary Science Reviews, 23(23-24), 2485-2500.

Speranza, F., Pompilio, M., Sagnotti, L., 2004. Paleomagnetism of spatter lavas from Stromboli volcano (Aeolian Islands, Italy): implications for the age of paroxysmal eruptions. Geophysical Research Letters, 31(2).

Speranza, F., Branca, S., Coltelli, M., D'Ajello Caracciolo, F., Vigliotti, L., 2006. How accurate is “paleomagnetic dating”? New evidence from historical lavas from Mount Etna. Journal of Geophysical Research: Solid Earth, 111(B12).

Speranza, F., Pompilio, M., D'Ajello Caracciolo, F., Sagnotti, L., 2008. Holocene eruptive history of the Stromboli volcano: constraints from paleomagnetic dating. Journal of Geophysical Research: Solid Earth, 113(B9).

Tanguy, J.C., Le Goff, M., Principe, C., Arrighi, S., Chillemi, V., Paiotti, A., Patanè, G., 2003. Archeomagnetic dating of Mediterranean volcanics of the last 2100 years: validity and limits. Earth and Planetary Science Letters, 211(1-2), 111-124.

Tomlinson, E.L., Thordarson, T., Müller, W., Thirlwall, M., Menzies, M.A., 2010. Microanalysis of tephra by LA-ICP-MS—Strategies, advantages and limitations assessed using the Thorsmörk ignimbrite (Southern Iceland). Chemical Geology, 279(3-4), 73-89.

Villasante-Marcos, V., Pavón-Carrasco, F.J., 2014. Palaeomagnetic constraints on the age of Lomo Negro volcanic eruption (El Hierro, Canary Islands). Geophysical Journal International, 199(3), 1497-1514.

Zanchetta, G., Sulpizio, R., Roberts, N., Cioni, R., Eastwood, W.J., Siani, G., Caron, B., Paterne, M., Santacroce, R., 2011. Tephrostratigraphy, chronology and climatic events of the Mediterranean basin during the Holocene: an overview. The Holocene, 21(1), 33-52.

Zijderveld, J.D.A., 1967. AC demagnetization of rocks: Analysis of results. In: Runcorn SK, Creer KM, Collinson DW (Eds.), Methods in Palaeomagnetism. Elsevier, Amsterdam, 254–286.

FIGURES

Figure 1. a) Sketch map showing the distribution of the main lithostratigraphic units targeted in the present study as obtained from the geological map of Lucchi et al. (2013). The studied outcrops and sampling sites are also indicated. In the inset, the location of the study area on Lipari and the position of the Lipari island in the Aeolian archipelago (Southern Italy) are shown. b) 3D image of the studied sector of Lipari (seen from NE) showing the main features and locations mentioned in the text (from https://www.terrametrics.com, ©2018 Google).

Figure 2. Outcrop photographs of the studied tephra units. a) Monte Pilato succession as exposed in the Porticello quarry (LIP03 in Figure 1a; a person in the foreground for scale). The red line marks the unconformity separating MP tephra from the upper RR activity. b) The MP tephra sequence in the Porticello quarry (LP1710 in Figure 1a, picture taken from the foreground ridge shown in (a); man for scale in the distal part of the rim, Panarea and Stromboli islands in the background). The very final (50 cm) part of the section belongs to the RR sequence. c) A portion of the Lami pyroclastic succession in one of the main outcrops near the vent area (LP1713 in Figure 1a). d) Upper part of the Rocche Rosse pyroclastic succession as visible at the top of the subvertical wall of the Porticello quarry (LP1704 in Figure 1a) showing the welded, darker pumice deposits on top of the sequence. RR lava on the foreground. e) Forgia Vecchia

pyroclastic succession (with the basal palaeosol) in an outcrop near Pirrera (LP1704 in Figure 1a).

Figure 3. The Monte Pilato pyroclastic succession. a) Synthetic stratigraphic succession based on the LP1710 and LP1714 outcrops, located within the crater and 1 km N, respectively (Fig. 1a); including grain-size distributions and componentry. b) Major and trace element glass compositions (hollow symbols refer to data from the other tephra units documented in this paper). c) Texture of the juvenile fragments (sample LP1714b) as seen in backscattered electron images.

Figure 4. The Forgia Vecchia pyroclastic succession. a) Stratigraphic succession at locality LP1704, located ~600 m north of the vent (Fig. 1a), including grain-size distributions and componentry. b) Major and trace element glass compositions (hollow symbols refer to data from the other studied tephra units). c) Texture of the juvenile fragments (sample LP1704c in backscattered electron images.

Figure 5. The Rocche Rosse pyroclastic succession. a) Synthetic stratigraphic succession based on observations within the Porticello quarry, grain-size distributions and componentry at LP1702 (Fig. 1a). b) Major and trace element glass compositions (hollow symbols refer to data from the other studied tephra units). c) Texture of the juvenile fragments in sample LP1702b as seen in backscattered images.

Figure 6. The Lami pyroclastic succession. a) Synthetic stratigraphic succession, grain-size distributions and componentry (LP1712 and LP1713; Fig. 1a). b) Major and trace element glass compositions (hollow symbols refer to data from the other studied tephra units). c) Texture of the juvenile fragments (sample LP1713d) as seen in backscattered electron images.

Figure 7. a) Equal-area projection (lower hemisphere) of site-mean paleomagnetic directions from the analyzed units. The ellipses around the palaeomagnetic directions are the projections of the relative α_{95} cones. All the paleomagnetic directions are listed in Table 3. b) Synthetic framework of the dating (^{14}C and paleomagnetic) obtained in the present study.^{14}C dates are reported at 95.4% confidence interval.

Figure 8. Main features (thickness and 2D-3D textures of the grains) of the distal rhyolitic Lipari-sourced tephra layers found in Stromboli (~40 km from Monte Pilato) and Vulcano (in an outcrop on Vulcanello; ~10 km from Monte Pilato) islands with their suggested dispersal on the basis of the proposed proximal-distal correlations.

Figure 9. Proximal-distal tephra correlations of the Lipari eruptions. Backscattered electron images of glass fragments in: (a) the proximal Monte Pilato pyroclastic succession; (b) Rocche Rosse proximal tephra; and the white tephra on (c) Stromboli and (d) Vulcanello. (e-g) Major and trace elements glass data from the distal tephra layers are the four studied proximal units on Lipari. Glass compositions of the 8.7-8.4 ka Vallone del Gabellotto pumiceous pyroclastic succession are shown for comparison. These older deposits have trace element glass compositions that are distinctly different from those of the recent Lipari activity.

Figure 10. Correlation of the stratigraphic successions and the reconstructed chrono-stratigraphic framework of the four eruptions during the last eruptive cycle of Lipari, based on stratigraphic relationships, and ^{14}C and paleomagnetic ages.

SUPPLEMENTARY FIGURES AND TABLES

Figure S1. Normalised to primitive mantle glass analyses for the studied Lipari events. The complete dataset is presented in Table S1.

Figure S2. Representative orthogonal vector diagrams of typical alternating field demagnetization data, in situ coordinates. Open and solid dots represent projections on the vertical and horizontal planes, respectively. Demagnetization step values are in mT.

Figure S3. Paleomagnetic dates of Lipari samples according to the method and software by Pavón-Carrasco et al. (2011), and the paleo-secular variation (PSV) reference model by Pavón-Carrasco et al. (2021). PSV curves for the declination, inclination and intensity are shown as thick red lines (thin red lines for the associated errors, 95% confidence level), together with the probability density curves (in grey-shade below each PSV). Palaeomagnetic declination, inclination and intensity values are shown in the PSV graphs as blue straight lines; the green dashed lines above and below are the 95% associated errors. The final combined probability density curves are shown in grey-shade (the 95% confidence level is shown as a green line).

Table S1. Complete dataset of normalized major and minor element glass compositions of tephra units from Lipari and for the two white tephra layers sampled at Stromboli and Vulcano islands. Totals reflect pre-normalised analytical totals. Analytical total and number of analyses (*n*) are also provided.

Table S2. Radiocarbon dates for the Forgia Vecchia charcoals and the recalibrated Keller (2002) dates. The determinations were calibrated in OxCal v4.4 (Ramsey et al., 2009) using the IntCal20 calibration curve (Reimer et al., 2020). Data are presented in calendar years AD.

Table 1. Sedimentological (grain-size statistical parameters and componentry) characteristics of the analyzed samples. Location coordinates for each sample are also reported.

		Location UTM		Grain size characteristics				Components (wt.%)				
Sample	**Eruption**	**Latitude**	**Longitude**	**Md_Φ**	**σ_Φ**	**S_{KI}**	**K_G**	**Obsidian**	**Highly vesicular pumice**	**Weakly vesicular pumice**	**Andesitic lithics**	**Rhyolitic lithics**
LP1701A	Rocche Rosse	38.30314N	14.37141E	-4.08	1.51	-1.51	1.24	33.3	-	66.4	0.2	-
LP1701B	Rocche Rosse	38.30314N	14.37141E	-2.46	1.63	-1.24	1.01	39.6	-	57.5	0.2	2.7
LP1702A	Rocche Rosse	38.30314N	14.37141E	0.58	2.31	1.24	0.84	15.76	-	76.8	7.44	-
LP1702B	Rocche Rosse	38.30314N	14.37141E	-2.85	2.11	-0.7	0.91	21.7	-	73.4	4.2	0.7
LP1702C	Rocche Rosse	38.30314N	14.37141E	-3.34	1.97	-0.87	0.96	9.1	-	88.6	1.8	0.6
LP1702D	Rocche Rosse	38.30314N	14.37141E	0.22	1.42	-0.66	1	9	-	91	-	-
LP1702E	Rocche Rosse	38.30314N	14.37141E	-0.97	3.05	-0.43	0.83	19.7	-	73.97	2.68	3.75
LP1702F	Rocche Rosse	38.30314N	14.37141E	2.15	3.02	0.22	0.78	1.63	-	80.07	18.3	-
LP1703A	Monte Pilato	38.29574N	14.36440E	-1.03	2.67	0.17	1.05	1.02	73	-	25.98	-
LP1703B	Monte Pilato	38.29574N	14.36440E	2.77	2.76	0.61	0.74	3.52	75.64	-	20.79	-
LP1704B	Forgia Vecchia	38.29401N	14.56575E	1.31	2.49	0.58	0.9	-	56.7	-	43.3	-
LP1704C	Forgia Vecchia	38.29401N	14.56575E	-2.94	1.5	-1.6	1.24	4.88	65.9	-	29.22	-
LP1704D	Forgia Vecchia	38.29401N	14.56575E	-2.01	2.12	-0.42	0.97	13.18	75.11	-	11.71	-
LP1704E	Forgia Vecchia	38.29401N	14.56575E	-2.47	1.93	-0.77	1.09	10.41	69.86	-	19.44	0.3
LP1706A	Forgia Vecchia	38.29168N	14.37153E	-0.86	1.47	-0.41	1.07	-	19.98	77.34	2.67	-
LP170	Forgia	38.2928	14.5657	-	1.3	-	1.75	1.16	94.46	-	0.4	3.99

7A	Vecchia	8N	0E	4.16	6	1.87						
LP1708A	Lami	38.49794N	14.95144E	-1.57	2.44	-0.34	0.87	12.8	86	-	0.75	-
LP1708B	Lami	38.49794N	14.95144E	-0.93	3.72	0.52	0.58	0.23	97.18	-	2.6	-
LP1708C	Lami	38.49794N	14.95144E	-2.19	2.5	-0.42	0.9	44.65	33.87	-	1.74	19.73
LP1709A	Lami	38.29483N	14.37091E	-3.35	1.61	-1.53	1.03	31.25	0.77	65.31	2.76	-
LP1710A	Monte Pilato	38.30165N	14.57039E	4.55	1.14	3.58	1.66	8	92	-	-	-
LP1710B	Monte Pilato	38.30165N	14.57039E	1.6	3.41	0.46	0.67	3.62	87.1	-	3.26	6.02
LP1710C	Monte Pilato	38.30165N	14.57039E	-0.87	2.71	0.41	1.32	14.49	84.05	-	1.13	0.33
LP1711A	Monte Pilato	38.30165N	14.57039E	-1.81	3.6	0.43	0.75	3.71	93.91	-	2.35	-
LP1713A	Lami	38.29530N	14.57073E	-3.7	2.72	-0.06	0.85	20.57	75.35	-	1.01	3.07
LP1713B	Lami	38.29530N	14.57073E	2.58	2.74	0.5	0.93	1.27	83.68	-	-	15.05
LP1713C	Lami	38.29530N	14.57073E	-3.05	1.67	-0.95	1.45	22.77	66.43	-	0.34	10.45
LP1713D	Lami	38.29530N	14.57073E	-2.39	1.75	-0.84	0.93	19.69	67.56		6.4	6.35
LP1713E	Lami	38.29530N	14.57073E	-0.5	3.23	0.58	0.6	2.25	-	85.14	12.61	-
LP1713F	Lami	38.29530N	14.57073E	-0.51	2.91	0.46	0.67	6.95	6.38	70.96	15.72	-
LP1714A	Monte Pilato	38.51536N	14.94714E	-1.69	3.11	0.18	0.73	-	94.58	-	5.36	0.06
LP1714B	Monte Pilato	38.51536N	14.94714E	-1.76	3.26	0.42	0.96	-	87.61	-	10.66	1.73
LP1714C	Monte Pilato	38.51536N	14.94714E	-2.98	3.14	0.04	0.96	0.11	66.25	-	32.37	1.26
LP1714D	Monte Pilato	38.51536N	14.94714E	-1.42	3.39	0.37	0.65	-	88.89	-	11.11	-
LP1714E	Monte Pilato	38.51536N	14.94714E	-2.75	3.81	0.35	0.81	0.06	96.59	-	3.35	-
LP1714F	Monte Pilato	38.51536N	14.94714E	-2.75	3.63	0.57	0.9	2.54	95.38	-	2.04	-
LP1715A	Monte Pilato	38.51536N	14.94714E	-1.5	3.31	0.5	0.81	0.45	93.27	-	6.28	-
LP1715B	Monte Pilato	38.51536N	14.94714E	-2.25	3.52	0.2	0.62	0.37	97.43	-	2.2	-
LP1715C	Monte Pilato	38.51536N	14.94714E	-3.09	3.92	0.55	0.61	-	98.25	-	1.75	-
LP171	Monte	38.5153	14.9471	-	3.6	0.3	0.78	4.91	-	68.72	26.37	-

5D	Pilato	6N	4E	2.32	4	2						
LP1716A	Rocche Rosse	38.30161N	14.57432E	-2.66	1.78	-1.22	1	4.96	-	91.5	2.99	0.55
LP1716B	Rocche Rosse	38.30161N	14.57432E	-3.27	1.72	1.13	1.05	34.5	-	63.74	1.68	0.07
LP1716C	Rocche Rosse	38.30161N	14.57432E	-3.45	1.48	-1.77	0.9	33.99	-	63.68	2	0.33

Table 2. Representative normalized major and minor element glass compositions of tephra units from Lipari and for the two white tephra layers sampled at Stromboli and Vulcano islands. A complete geochemical dataset is provided in Table S1. Analytical totals and number of analyses (*n*) are also provided.

Eruption unit	**Monte Pilato (MP)**		**Forgia Vecchia (FV)**		**Rocche Rosse (RR)**		**Lami (LA)**		**White Tephra Vulcano**		**White Tephra Stromboli**	
wt.% (norm.)	Avg.	1σ	Avg.	1σ	Avg.	1σ	Avg.	1σ	Avg.	1σ	Avg.	1σ
SiO_2	74.83	0.22	75.38	0.21	74.81	0.44	75.30	0.18	74.90	0.14	74.98	0.14
TiO_2	0.08	0.03	0.08	0.03	0.08	0.03	0.07	0.02	0.08	0.03	0.07	0.02
Al_2O_3	13.09	0.20	12.75	0.12	13.18	0.36	12.77	0.17	13.15	0.10	13.11	0.11
FeOt	1.58	0.10	1.53	0.11	1.54	0.10	1.51	0.11	1.58	0.06	1.57	0.06
MnO	0.07	0.03	0.07	0.03	0.07	0.03	0.07	0.03	0.07	0.02	0.06	0.02
MgO	0.04	0.02	0.04	0.02	0.04	0.02	0.04	0.02	0.04	0.02	0.03	0.02
CaO	0.75	0.04	0.73	0.04	0.74	0.04	0.74	0.04	0.75	0.02	0.75	0.02
Na_2O	3.99	0.17	4.05	0.13	4.04	0.14	4.05	0.11	3.99	0.06	4.00	0.11
K_2O	5.20	0.11	5.00	0.08	5.13	0.12	5.07	0.11	5.07	0.07	5.03	0.07
P_2O_5	0.01	0.01	0.01	0.02	0.01	0.02	0.01	0.01	0.01	0.02	0.01	0.01
Cl	0.39	0.03	0.37	0.02	0.36	0.03	0.37	0.03	0.36	0.03	0.40	0.03
Na_2O+K_2O	9.19	0.18	9.05	0.14	9.18	0.17	9.12	0.10	9.06	0.08	9.02	0.09
Analytical Total	96.76	1.87	99.69	0.96	98.84	1.29	99.27	0.78	99.87	0.59	97.21	1.31
n	*128*		*80*		*114*		*50*		*29*		*25*	
(ppm)												
Rb	326.6	6.5	327.5	5.1	331.7	15.0	329.1	15.6	330.9	12.5	336.7	11.9
Sr	17.5	3.5	16.9	0.7	16.8	1.4	17.8	2.9	16.8	2.6	17.2	1.2
Y	39.2	2.1	40.6	0.7	40.3	0.9	40.7	1.1	41.0	0.8	38.7	1.6
Zr	178.2	8.6	184.0	2.9	182.2	3.5	183.6	4.6	186.8	2.9	176.1	7.2
Nb	38.8	0.9	39.2	0.6	39.3	0.8	39.4	0.7	38.6	0.5	38.7	1.5
Ba	17.6	1.6	17.7	0.4	17.5	1.0	17.9	0.9	17.6	1.5	21.3	5.5
La	63.3	3.7	65.6	1.1	65.1	1.3	65.5	1.5	66.6	1.0	62.8	2.7
Ce	123.9	5.9	127.1	2.1	126.6	2.4	127.9	3.1	127.8	2.1	122.8	5.9
Pr	12.5	0.6	12.8	0.2	12.7	0.2	12.8	0.3	13.0	0.2	12.4	0.6
Nd	43.2	2.1	44.6	1.0	44.5	1.1	44.8	1.1	45.3	1.4	43.6	2.0
Sm	8.4	0.5	8.8	0.2	8.7	0.3	8.7	0.3	8.9	0.4	8.3	0.5
Eu	0.2	0.0	0.2	0.0	0.2	0.0	0.2	0.0	0.1	0.0	0.2	0.0
Gd	6.5	0.4	6.8	0.2	6.8	0.2	6.8	0.2	6.9	0.3	6.5	0.3
Dy	6.7	0.4	6.9	0.2	6.9	0.2	6.9	0.2	7.1	0.3	6.4	0.6
Er	4.1	0.3	4.3	0.1	4.3	0.1	4.3	0.2	4.4	0.2	4.1	0.2
Yb	4.6	0.3	4.8	0.2	4.7	0.2	4.8	0.2	4.8	0.2	4.5	0.3
Lu	0.67	0.05	0.70	0.02	0.69	0.02	0.70	0.05	0.71	0.03	0.7	0.0
Hf	6.5	0.4	6.8	0.2	6.7	0.2	6.7	0.3	6.9	0.3	6.5	0.4
Ta	2.6	0.1	2.7	0.0	2.7	0.1	2.7	0.1	2.7	0.0	2.6	0.2
Th	52.7	3.0	54.8	1.0	54.2	1.2	54.6	1.5	55.9	0.9	51.5	3.2
U	16.7	0.5	16.9	0.3	16.9	0.4	17.0	0.4	16.8	0.3	16.3	0.9
n	*96*		*60*		*69*		*77*		*18*		*19*	

Table 3. Paleomagnetic direction and paleomagnetic dating from Lipari lava flows and welded pumices. Site coordinates were gathered by a Garmin GPS, using the WGS84 datum. n/Nis number of ChRM directions used to calculate the site-mean direction/total number of cores drilled at a site, or number of ChRM directions used to calculate the volcanic unit-mean direction/total number of cores drilled in the volcanic unit. D is paleomagnetic declination, I is inclination, k and α_{95} are statistical parameters after Fisher, (1953). Paleomagnetic ages were obtained by comparing the lava flow/welded pumice-mean paleomagnetic directions with the SCHA.DIF.4K paleo-secular variation regional model by Pavón-Carrasco et al. (2021), using the Matlab software of Pavón-Carrasco et al. (2011). Paleomagnetic direction (1) is from Arrighi et al. (2006). The Rocche Rosse lava flow age was obtained also using the lava paleointensity value (52.4±1.1μT) reported by Leonhardt et al. (2006). *discarded sites with scattered ChRMs. §Preferred age for the Rocche Rosse eruption (see text).

Volcanic Unit	Code	n/N	Latitude, °N	Longitude, °E	D, deg	I, deg	k	α_{95}, deg	Paleomagnetic dating (yr AD)
Forgia Vecchia Lava Flow	LIP01*	10/10	38°29'14.1"	14°56'59.0	5.1	10.7	2.6	37.8	
Forgia Vecchia Lava Flow	LIP02	9/10	38°29'13.7"	14°56'59.5"	17.0	29.0	168.5	4.0	1242-1306
Forgia Vecchia Lava Flow	LIP06*	10/10	38°29'33.2"	14°57'33.4"	7.9	31.0	5.5	22.6	
Rocche Rosse Welded Pumice	LIP03	11/13	38°30'37.5"	14°57'11.7"	4.3	52.9	154.9	3.7	
Rocche Rosse Welded Pumice	LIP04	9/12	38°30'38.2"	14°57'11.8"	3.5	51.4	79.19	5.8	
	Sample mean (LIP03+LIP04)	20/25			3.9	52.2	113.4	3.1	1329-1417 1420-1490

Lami Welded Pumice	LIP05	15/16	38°29'49.2"	14°57'08.9"	11.9	36.0	118.6	3.5	1253-1316 1392-1410
Rocche Rosse Lava Flow	LIP07	9/10	38°31'06.6"	14°56'53.9"	11.4	39.2	84.06	5.6	
Rocche Rosse Lava Flow	LIP08	8/10	38°31'11.2"	14°56'52.7"	18.3	36.8	90.0	5.9	
	Sample mean (LIP07+LIP08)	17/20			14.7	38.1	82.0	4.0	1243-1304 (§)
Rocche Rosse Lava Flow (1)	LP1	17/26			15.9	47.9	327	1.8	1183-1274

Site coordinates were gathered by a Garmin GPS, using the WGS84 datum. n/N is number of ChRM directions used to calculate the site-mean direction /total number of cores drilled at a site, or number of ChRM directions used to calculate the volcanic unit-mean direction /total number of cores drilled in the volcanic unit. D is paleomagnetic declination, I is inclination, k and α_{95} are statistical parameters after Fisher, (1953). Paleomagnetic ages were obtained by comparing the lava flow/welded pumice-mean paleomagnetic directions with the SCHA.DIF.4K paleo-secular variation regional model by Pavón-Carrasco et al. (2021), using the Matlab software of Pavón-Carrasco et al. (2011). Paleomagnetic direction (1) is from Arrighi et al. (2006). The Rocche Rosse lava flow age was obtained also using the lava paleointensity value (52.4±1.1 μT) reported by Leonhardt et al. (2006). * discarded sites with scattered ChRMs. § Preferred age for the Rocche Rosse eruption (see text).

Highlights

- Stratigraphy of tephra and lavas of post-1500 yrs activity of Lipari was studied
- Stratigraphy was combined with paleomagnetic and ^{14}C dates and historical reports
- The rhyolitic ash found on Stromboli is attributed to Monte Pilato eruption
- The ash bed dispersed at La Fossa of Vulcano is consistent with Rocche Rosse eruption
- We suggest a likely correlation with Forgia Vecchia for an ash bed of the Ionian Sea

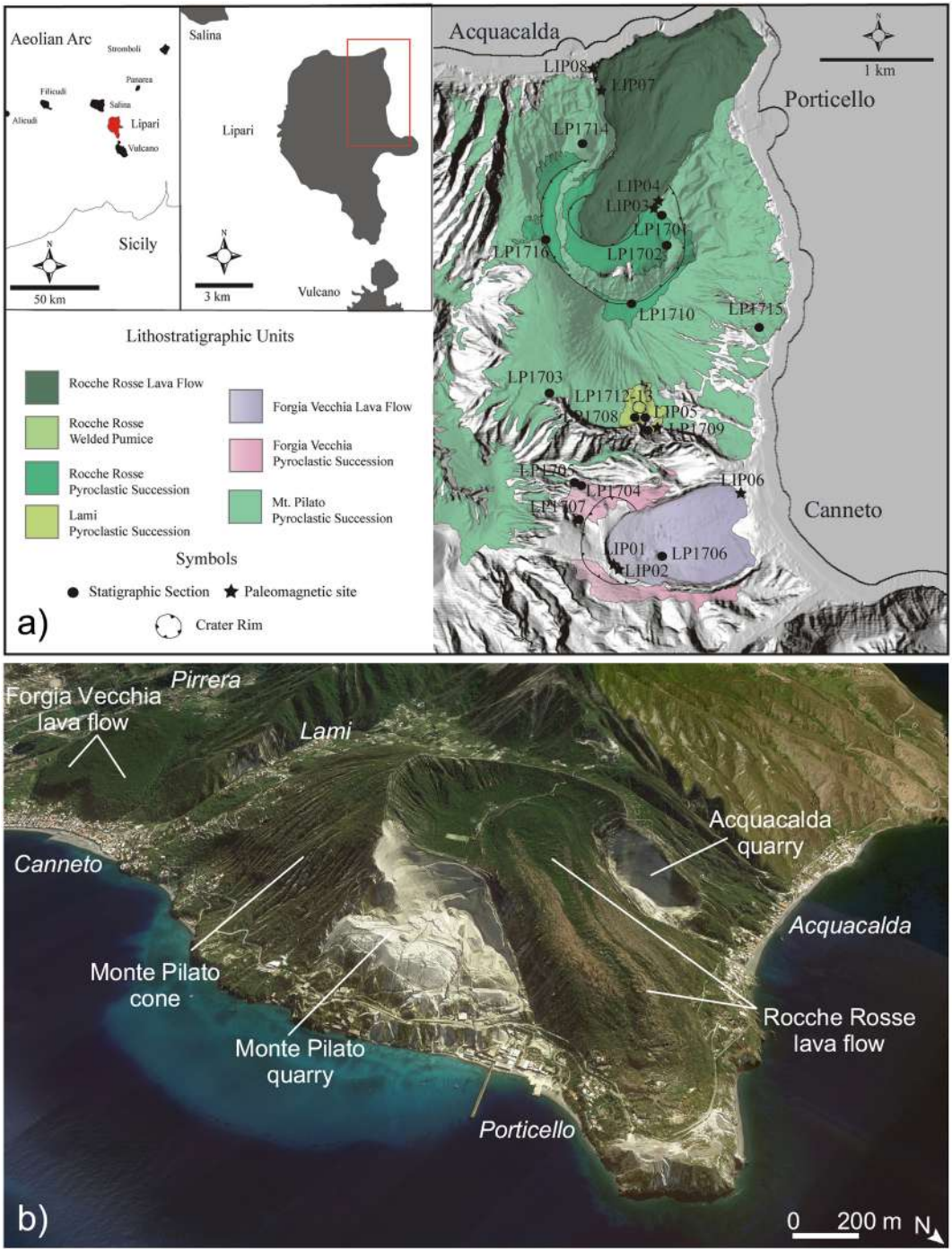
Aeolian Arc
Stromboli
Panarea
Filicudi
Salina
Alicudi
Lipari
Vulcano
Sicily
50 km
Salina
Lipari
3 km
Vulcano
Acquacalda
Porticello
Canneto
1 km
LIP08
LIP07
LP1714
LIP04
LIP03
LP1701
LP1716
LP1702
LP1710
LP1715
LP1703
LP1712-13
LP1708
LIP05
LP1709
LP1705
LP1704
LIP06
LP1707
LIP01
LP1706
LIP02
Lithostratigraphic Units
Rocche Rosse Lava Flow
Rocche Rosse Welded Pumice
Rocche Rosse Pyroclastic Succession
Lami Pyroclastic Succession
Forgia Vecchia Lava Flow
Forgia Vecchia Pyroclastic Succession
Mt. Pilato Pyroclastic Succession
Symbols
Statigraphic Section
Paleomagnetic site
Crater Rim
a)
Forgia Vecchia lava flow
Pirrera
Lami
Canneto
Acquacalda quarry
Acquacalda
Monte Pilato cone
Monte Pilato quarry
Rocche Rosse lava flow
Porticello
b)
0 200 m
N

Figure 1

Figure 2

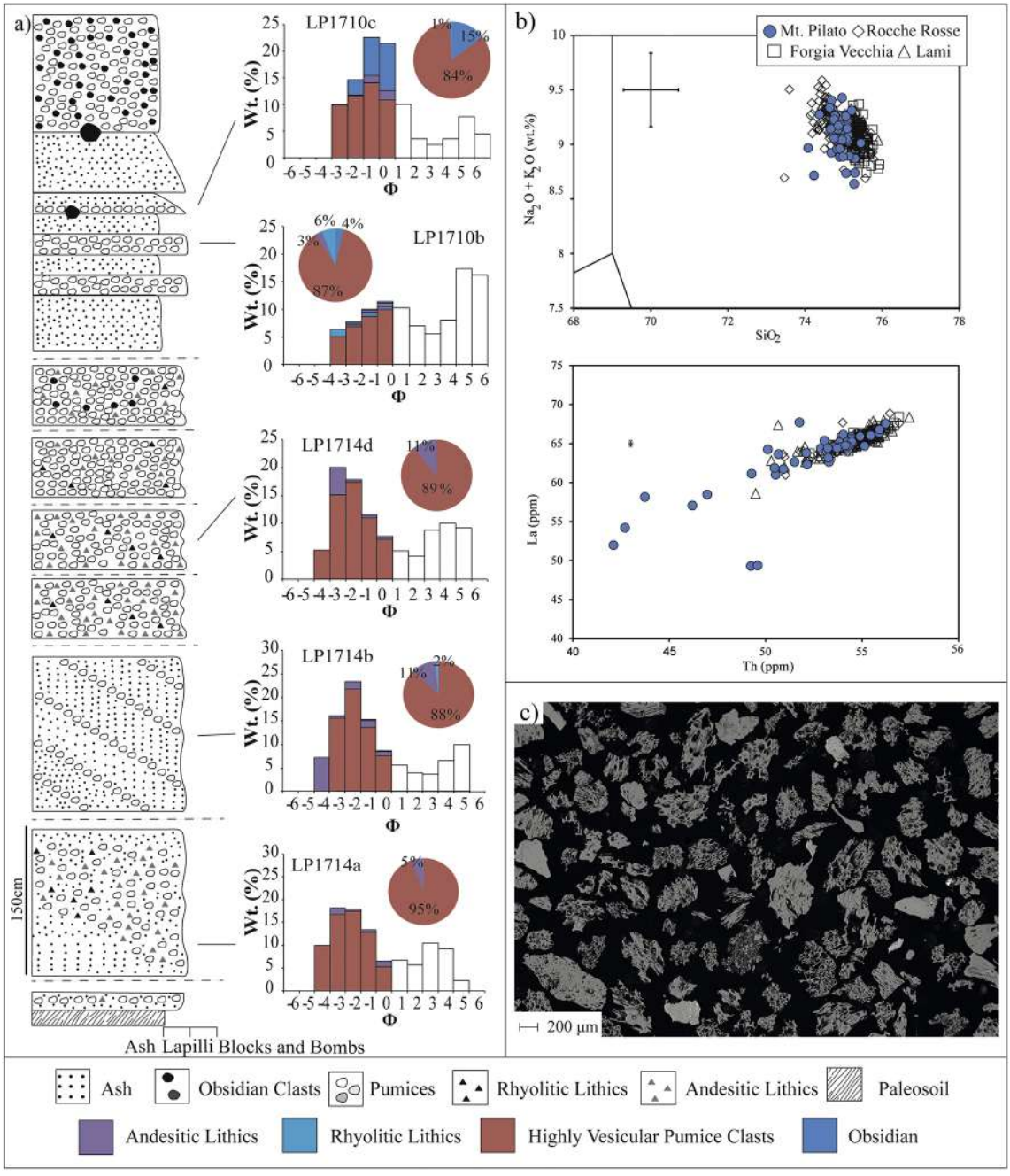
a)
LP1710c
1%
15%
84%
Wt. (%)
Φ
LP1710b
6%
4%
3%
87%
LP1714d
11%
89%
LP1714b
2%
11%
88%
LP1714a
5%
95%
150cm
Ash Lapilli Blocks and Bombs
b)
Mt. Pilato ◇Rocche Rosse
Forgia Vecchia △ Lami
Na2O + K2O (wt.%)
SiO2
La (ppm)
Th (ppm)
c)
200 µm
Ash
Obsidian Clasts
Pumices
Rhyolitic Lithics
Andesitic Lithics
Paleosoil
Andesitic Lithics
Rhyolitic Lithics
Highly Vesicular Pumice Clasts
Obsidian

Figure 3

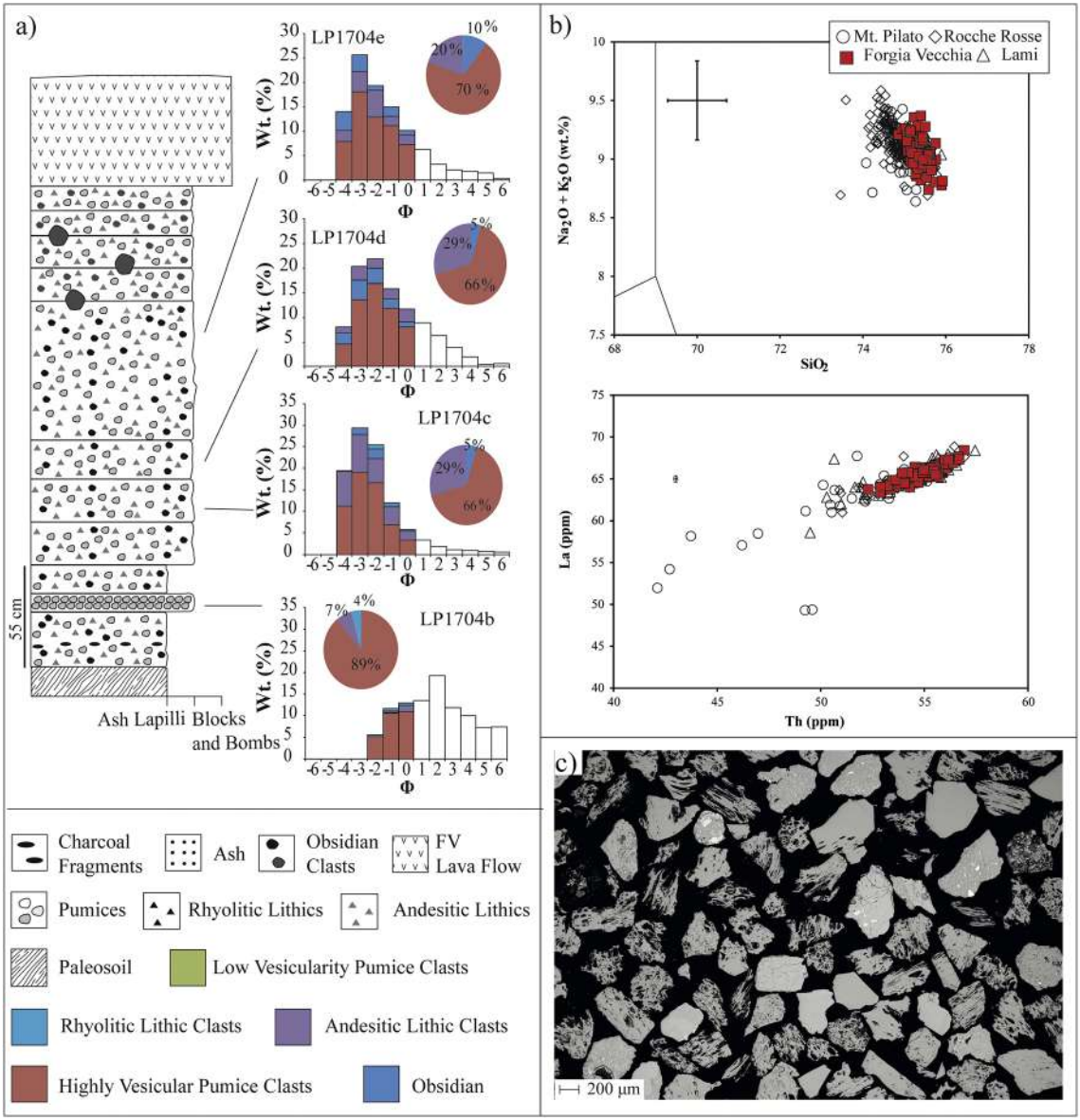
a)
LP1704e
10%
20%
70 %
LP1704d
5%
29%
66%
LP1704c
5%
29%
66%
LP1704b
7%
4%
89%
Wt. (%)
Φ
55 cm
Ash Lapilli Blocks and Bombs
Charcoal Fragments
Ash
Obsidian Clasts
FV Lava Flow
Pumices
Rhyolitic Lithics
Andesitic Lithics
Paleosoil
Low Vesicularity Pumice Clasts
Rhyolitic Lithic Clasts
Andesitic Lithic Clasts
Highly Vesicular Pumice Clasts
Obsidian
b)
Mt. Pilato
Rocche Rosse
Forgia Vecchia
Lami
Na2O + K2O (wt.%)
SiO2
La (ppm)
Th (ppm)
c)
200 µm

Figure 4

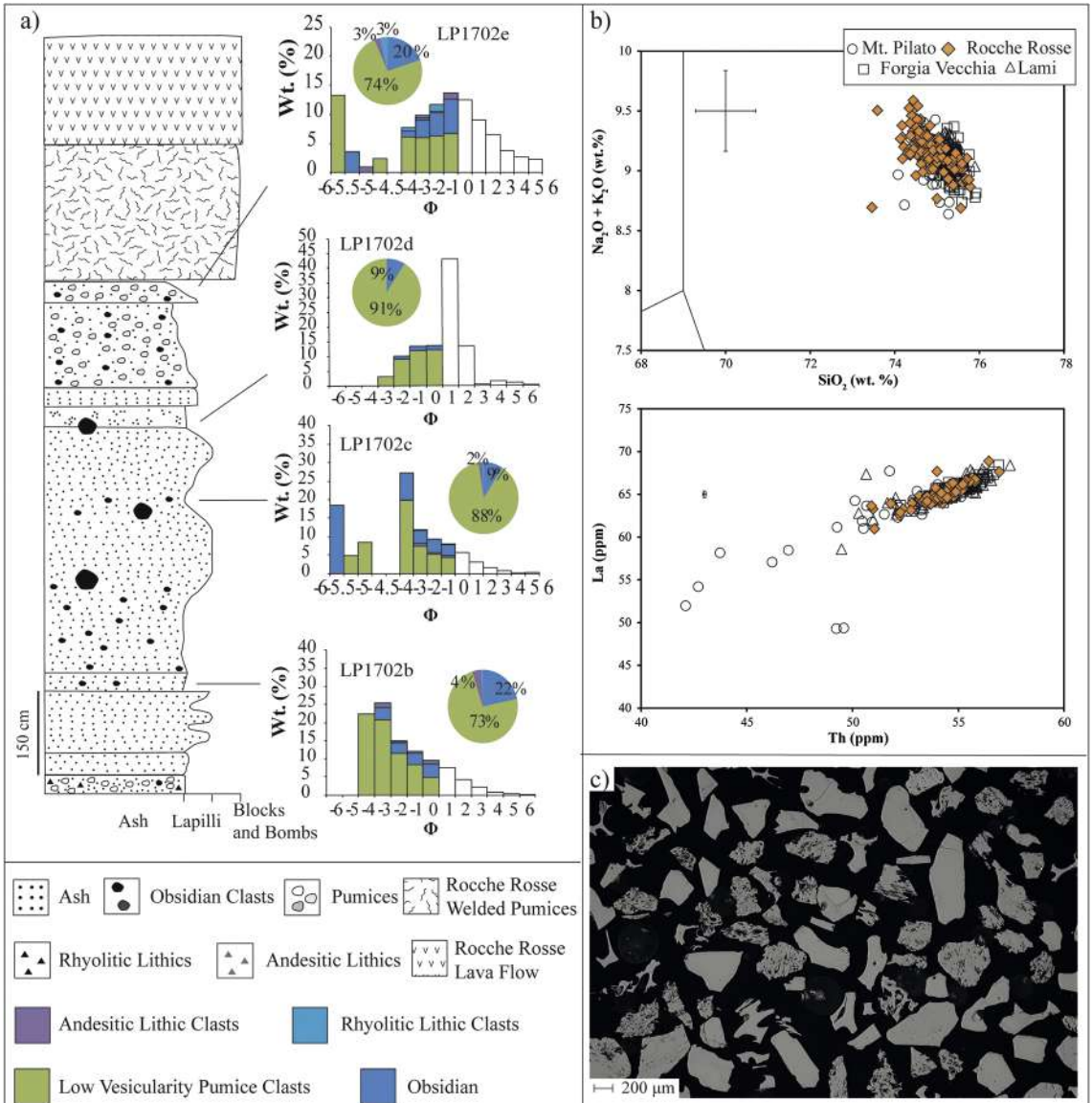
a)
LP1702e
3%
3%
20%
74%
Wt. (%)
Φ
LP1702d
9%
91%
LP1702c
2%
9%
88%
LP1702b
4%
22%
73%
150 cm
Ash
Lapilli
Blocks and Bombs
Ash
Obsidian Clasts
Pumices
Rocche Rosse Welded Pumices
Rhyolitic Lithics
Andesitic Lithics
Rocche Rosse Lava Flow
Andesitic Lithic Clasts
Rhyolitic Lithic Clasts
Low Vesicularity Pumice Clasts
Obsidian
b)
Mt. Pilato
Rocche Rosse
Forgia Vecchia
Lami
Na2O + K2O (wt.%)
SiO2 (wt. %)
La (ppm)
Th (ppm)
c)
200 µm

Figure 5

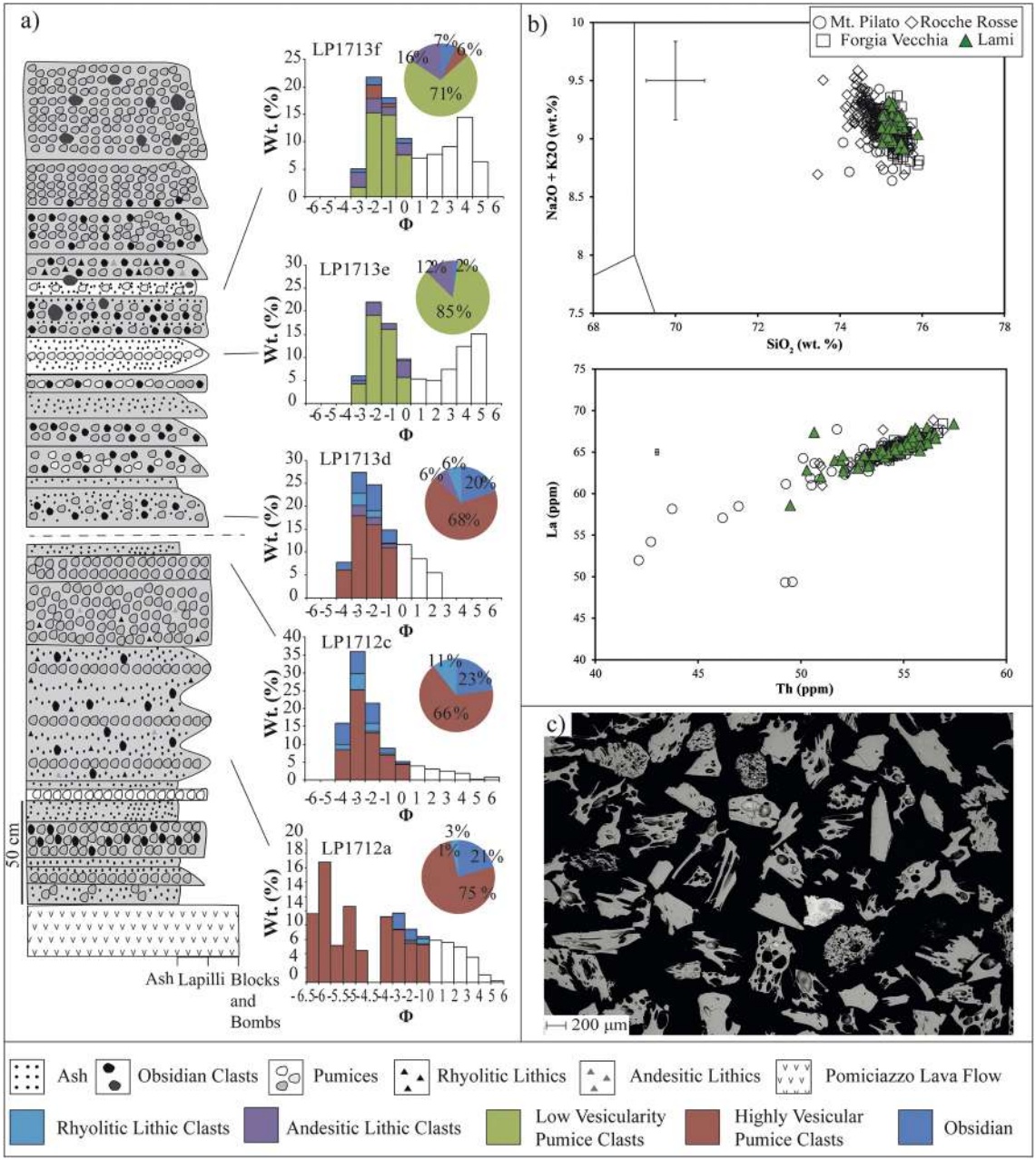
a)
LP1713f
16%
7%
6%
71%
Wt. (%)
Φ
LP1713e
12%
2%
85%
LP1713d
6%
6%
20%
68%
LP1712c
11%
23%
66%
LP1712a
3%
1%
21%
75 %
50 cm
Ash Lapilli Blocks and Bombs
b)
Mt. Pilato
Rocche Rosse
Forgia Vecchia
Lami
Na2O + K2O (wt.%)
SiO2 (wt. %)
La (ppm)
Th (ppm)
c)
200 µm
Ash
Obsidian Clasts
Pumices
Rhyolitic Lithics
Andesitic Lithics
Pomiciazzo Lava Flow
Rhyolitic Lithic Clasts
Andesitic Lithic Clasts
Low Vesicularity Pumice Clasts
Highly Vesicular Pumice Clasts
Obsidian

Figure 6

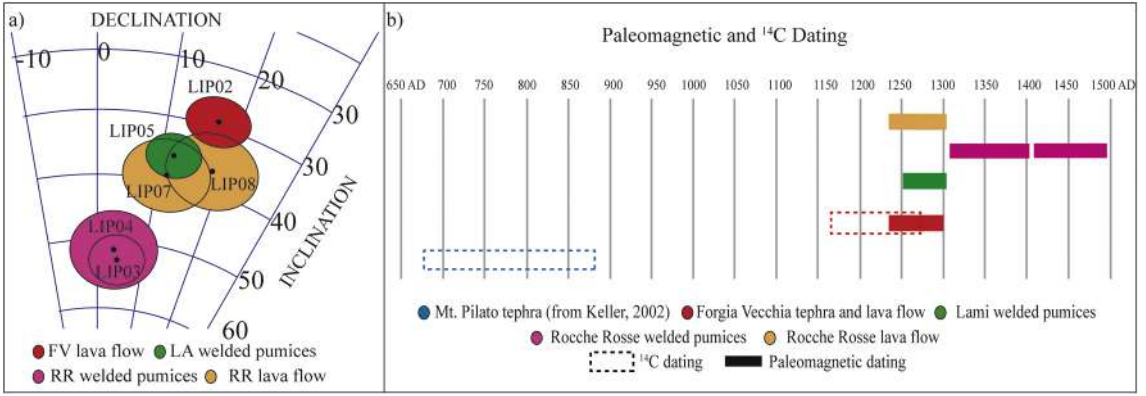
a)
DECLINATION
-10
0
10
20
30
40
50
60
INCLINATION
LIP02
LIP05
LIP07
LIP08
LIP04
LIP03
FV lava flow
LA welded pumices
RR welded pumices
RR lava flow
b)
Paleomagnetic and 14C Dating
650 AD
700
750
800
850
900
950
1000
1050
1100
1150
1200
1250
1300
1350
1400
1450
1500 AD
Mt. Pilato tephra (from Keller, 2002)
Forgia Vecchia tephra and lava flow
Lami welded pumices
Rocche Rosse welded pumices
Rocche Rosse lava flow
14C dating
Paleomagnetic dating

Figure 7

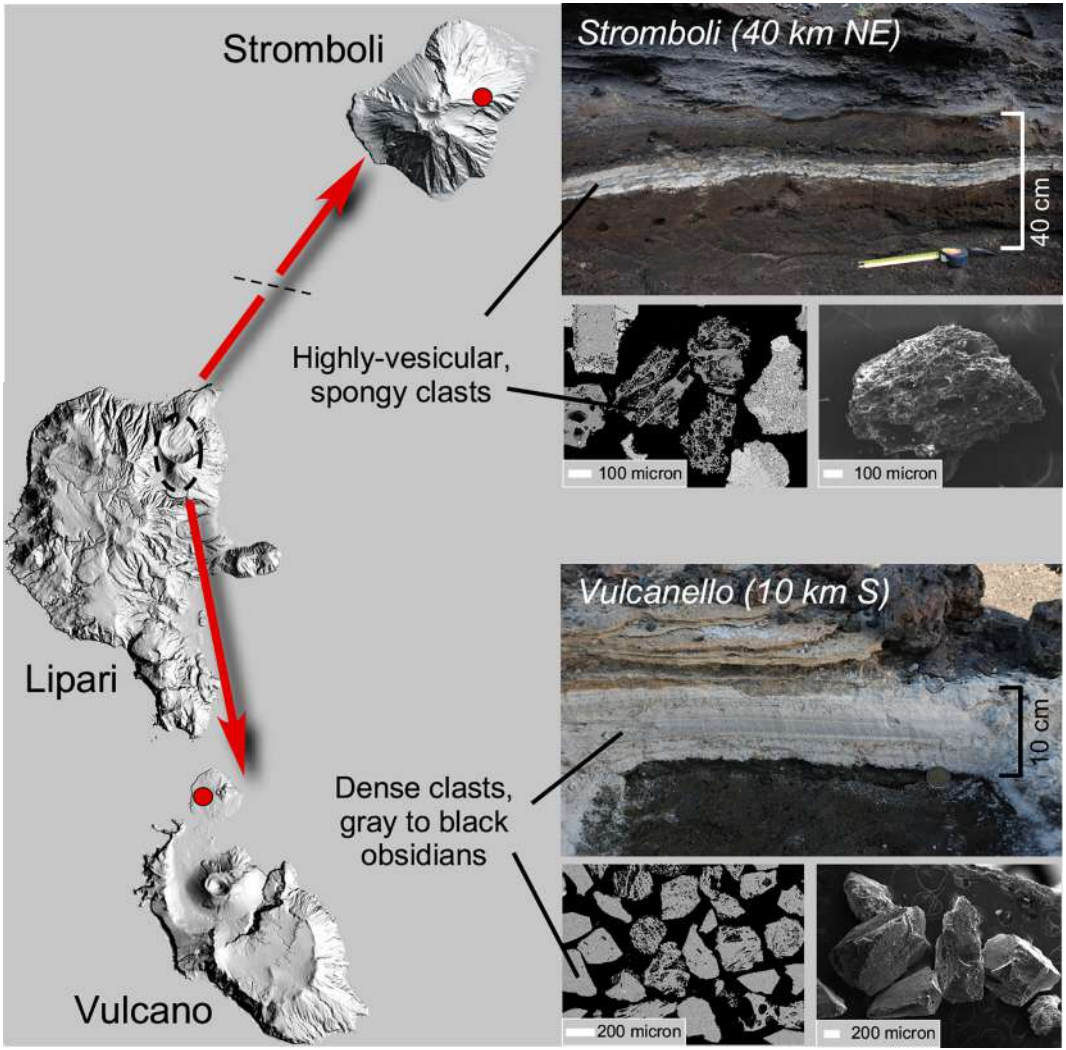
Stromboli
Stromboli (40 km NE)
40 cm
Highly-vesicular,
spongy clasts
100 micron
100 micron
Lipari
Vulcanello (10 km S)
10 cm
Dense clasts,
gray to black
obsidians
200 micron
200 micron
Vulcano

Figure 8

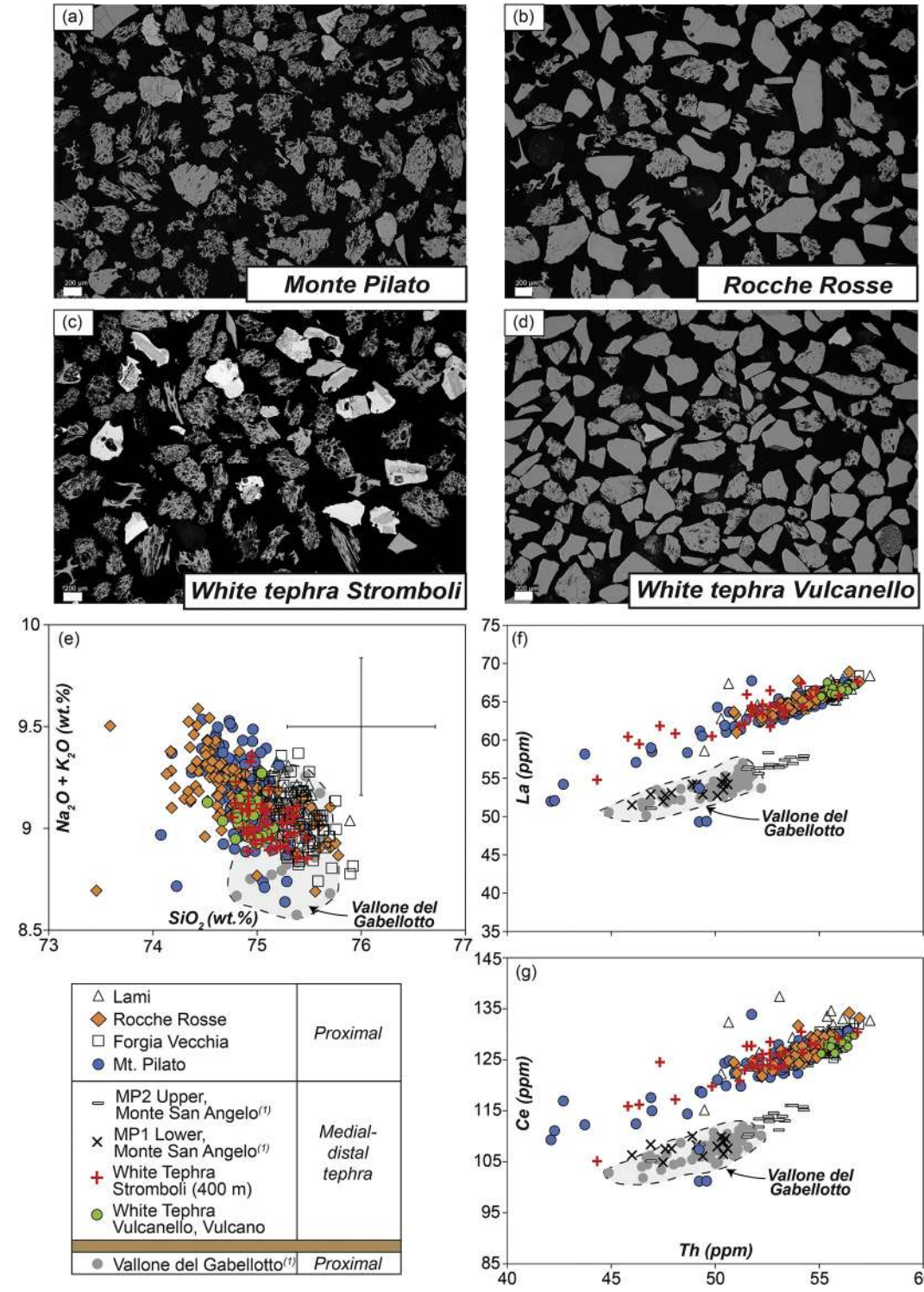
(a)
Monte Pilato
(b)
Rocche Rosse
(c)
White tephra Stromboli
(d)
White tephra Vulcanello
(e)
$Na_2O + K_2O$ (wt.%)
SiO_2 (wt.%)
Vallone del Gabellotto
(f)
La (ppm)
Vallone del Gabellotto
(g)
Ce (ppm)
Th (ppm)
Vallone del Gabellotto
Lami
Rocche Rosse
Forgia Vecchia
Mt. Pilato
Proximal
MP2 Upper, Monte San Angelo(1)
MP1 Lower, Monte San Angelo(1)
White Tephra Stromboli (400 m)
White Tephra Vulcanello, Vulcano
Medial-distal tephra
Vallone del Gabellotto(1)
Proximal

Figure 9

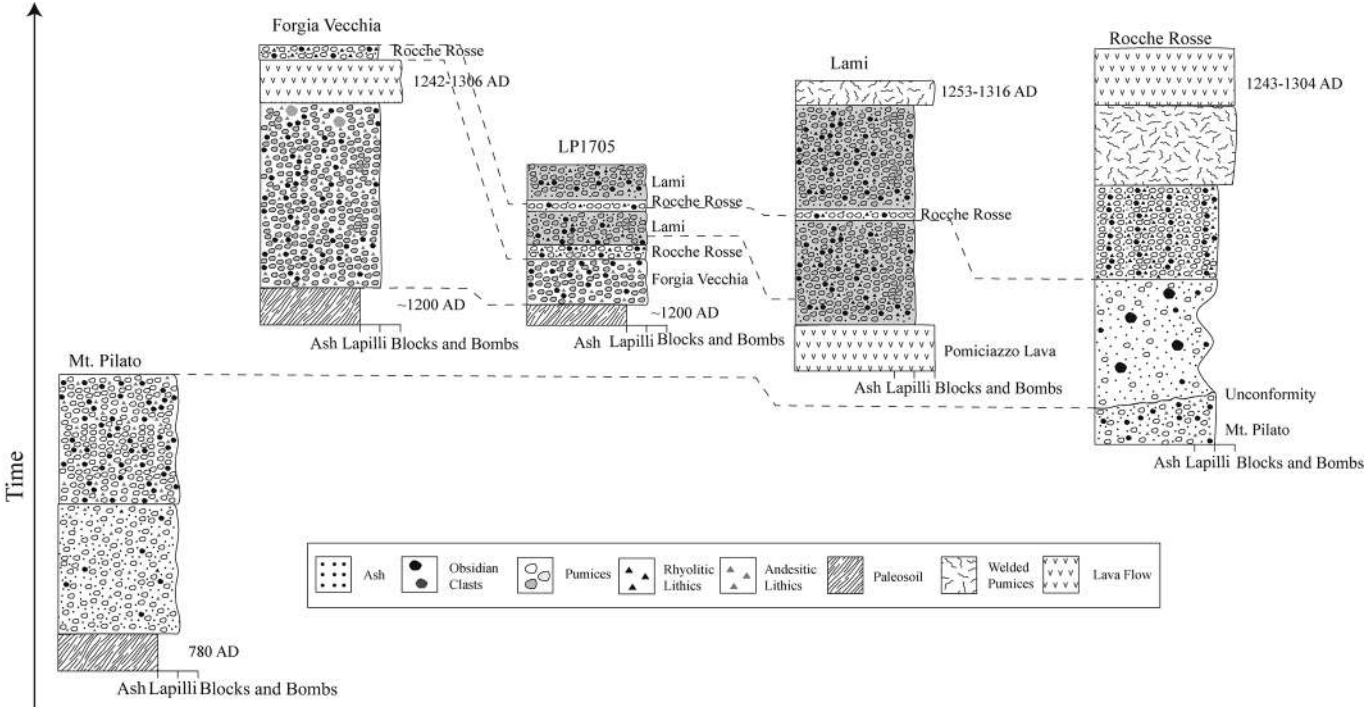
Time
Forgia Vecchia
Rocche Rosse
1242-1306 AD
~1200 AD
Ash Lapilli Blocks and Bombs
LP1705
Lami
Rocche Rosse
Lami
Rocche Rosse
Forgia Vecchia
~1200 AD
Ash Lapilli Blocks and Bombs
Lami
1253-1316 AD
Rocche Rosse
Pomiciazzo Lava
Ash Lapilli Blocks and Bombs
Rocche Rosse
1243-1304 AD
Unconformity
Mt. Pilato
Ash Lapilli Blocks and Bombs
Mt. Pilato
780 AD
Ash Lapilli Blocks and Bombs
Ash
Obsidian Clasts
Pumices
Rhyolitic Lithics
Andesitic Lithics
Paleosoil
Welded Pumices
Lava Flow

Figure 10